p38α kinase inhibition for the treatment of colorectal cancer

Dissertation

der Mathematisch-Naturwissenschaftlichen Fakultät

der Eberhard Karls Universität Tübingen

zur Erlangung des Grades eines

Doktors der Naturwissenschaften

(Dr. rer. nat.)

vorgelegt von

M.Sc. Jule Harbig

aus Oberkirch

Tübingen

2021

Gedruckt mit Genehmigung der Mathematisch-Naturwissenschaftlichen Fakultät der Eberhard Karls Universität Tübingen.

Tag der mündlichen Qualifikation:	02.02.2022
Dekan:	Prof. Dr. Thilo Stehle
1. Berichterstatter:	Prof. Dr. Stefan Laufer
2. Berichterstatter:	Prof. Dr. Lars Zender

Table of contents

Abbreviations

2D	Two-dimensional
3D	Three-dimensional
AOM	Azoxymethane
APC	Adenomatous polyposis coli
APS	Ammonium persulfate
ASC	Adult stem cell
ATF2	Activating transcription factor 2
BAP	Braf – Apc – p53
CAC	Colitis-associated cancer
Cas9	CRISPR associated protein 9
CBC	Crypt base columnar
CDC25	Cell division cycle 25
CDK1	Cyclin-dependent kinase 1
CHOP	C/EBP homologous protein
CIMP	The CpG island methylator phenotype
CIP	Calf Intestinal Alkaline Phosphatase
CK20	Cytokeratin 20
CNV	Copy number variation
CRC	Colorectal cancer
CRISPR	clustered regularly interspaced short palindromic repeats
CTG	Cell Titer Glo
CTLA-4	cytotoxic T-lymphocyte-associated protein 4
DAPI	4′,6-diamidino-2-phenylindole
DMEM	Dulbecco's modified Eagle's medium
DMSO	Dimethyl sulfoxide
DNA	Deoxyribonucleic acid
DSS	Dextran sulfate sodium
DTT	Dithiothreitol
EDTA	Ethylenediaminetetraacetic acid
EdU	5-Ethynyl-2´-deoxyuridine
EGFR	Epidermal growth factor receptor
ENU	ethylnitrosourea
EtOH	Ethanol
FAP	Familial adenomatous polyposis
FCS	Fetal calf serum
GEMM	Genetically engineered mouse model
GFP	Green fluorescent protein
GFR	Growth Factor Reduced
H&E	Hematoxylin and eosin
HCC	Hepatocellular carcinoma
hCRC	Human colorectal cancer
HDI	Human Development Index
HGD	High-grade dysplasia
HNPCC	Hereditary nonpolyposis colorectal cancer
HSP27	Heat shock protein 27
IBD	Inflammatory bowel disease
IF	Immunofluorescence
IgG	Immunoglobulin G

IHC	Immunohistochemistry
IL	Interleukin
INDEL	Insertion/Deletion
iPSC	Induced pluripotent stem cell
KAP	Kras – Apc- p53
KMP	Kras – Myc – p53
KRAS	Kirsten rat sarcoma
LB	Lysogeny broth
LGD	Low-grade dysplasia
Lgr5	Leucine-rich repeat-containing G-protein coupled receptor 5
LPS	Lipopolysaccharide
MAPK	Mitogen-associated protein kinase
Min	multiple intestinal neoplasia
MLH1	MutL homolog 1
MMR	Mismatch repair
MSI	Microsatellite instability
NEB	New England Biolabs
NFKBIA	nuclear factor of kappa light polypeptide gene enhancer in B-cells inhibitor, alpha
NF-κB	nuclear factor kappa-light-chain-enhancer of activated B cells
NGS	Next-generation sequencing
NRAS	Neuroblastoma rat sarcoma
NT	Not transformed
PBS	Phosphate-buffered saline
NRAS	Neuroblastoma rat sarcoma
NT	Not transformed
PBS	Phosphate-buffered saline
PBST/TBST	+Tween
PCR	Polymerase chain reaction
PD-1	Programmed cell death protein 1
PDTO	Patient-derived tumor organoid
PDTX	Patient-derived tumor xenograft
PFS	Progression-free survival
PGE2	Prostaglandin E2
PH	PH797804
PIK3CA	phosphatidylinositol-4,5-bisphosphate 3-kinase
PK	Pharmacokinetics
PTEN	Phosphatase and tensin homolog
qRT-PCR	quantitative real-time PCR
RAF	Rapidly accelerated fibrosarcoma
RAS	Rat sarcoma
Ren	Renilla reniformis
RNA	Ribonucleic acid
RPMI	Roswell Park Memorial Institute

RT3GEPIR	TRE(3G) GFP miR-E PGK Puro IRES rtTA3
SDS	Sodium dodecyl sulfate
SDS-PAGE	sodium dodecyl sulfate polyacrylamide gel electrophoresis
sgRNA	single-guide RNA
shRNA	Short hairpin RNA
siRNA	Small interfering RNA
SKL	Skepinone-L
SNV	single nucleotide variant
SSA	Sessile serrated adenoma
STAT3	signal transducer and activator of transcription 3
TBS	Tris Buffered Saline
TCGA	The Cancer Genome Atlas
TEMED	Tetramethylethylenediamine
TGF	Transforming growth factor
TNF	Tumor necrosis factor
VEGF	Vascular endothelial growth factor
WES	Whole exome sequencing
WGO	World Gastroenterology Organisation
WT	Wildtype
IRES	Internal ribosome entry site
PGK	Phosphoglycerate kinase
TRE	Tetracycline response element
rtTA3	tetracycline-regulated transactivator gene
NCI	National Cancer Institute

Summary

p38α (Mapk14) is a member of the MAP kinase family and can be activated by environmental stress signaling and pro-inflammatory cytokines. Recent data suggest p38α as a potential target for the treatment of colitis-associated colorectal cancer (CRC). However, CRC that is linked to ulcerative colitis or to Crohn's disease accounts for only a small subgroup of cases.

In order to determine the therapeutic potential of p38α inhibition in colitis-independent colorectal cancer, I generated organoid-based CRC mouse models. Organoid cultures of murine colon epithelial cells were established and transformed *in vitro* by genetic modification of *Apc*, *Kras* and *Trp53* using CRISPR/Cas9 and *cre* recombinase. Upon transformation, these cultures were re-transplanted into mice where they efficiently formed colorectal tumors. By seeding organoid CRC cells into the spleen, I was able to generate tumor formation in the liver in order to model CRC metastases.

By using shRNA interference, I found that *Mapk14*/p38α represents an important factor in CRC development. However, treatment of organoid-based CRC models *in vitro* and *in vivo* with specific and well-established p38α inhibitors (Skepinone-L, PH797804), did not result in a pronounced therapeutic effect. Mechanistic studies revealed that increased activation of p38α kinase during therapy counteracts complete p38α pathway inhibition in CRC.

To allow for a full blockade of p38α a signaling in colorectal cancer, I tested a novel class of type 1.5 p38α inhibitors with picomolar activity and substantially improved target residence time that were generated by the Laufer Lab. I applied these inhibitors in different CRC organoid cultures and detected a strong therapeutic response due to induction of DNA damage and an altered G2/M checkpoint leading to cell death. These compounds are well tolerated by mice and efficiently block CRC development *in vivo*.

To determine the potential of novel p38α compounds with increased target residence time in human CRC, I generated a panel of patient-derived CRC organoid cultures. These cultures showed an initial resistance to standard chemotherapies and p38α

inhibition with established inhibitors; however, strongly respond to a treatment with our new generation p38α inhibitors.

Taken together, my data indicate that new generation p38α inhibitors with substantially improved target residence time have a therapeutic potential for the treatment of advanced colorectal cancer.

Zusammenfassung

p38α (Mapk14) gehört zur Familie der MAP-Kinasen und kann u.a. durch Stresssignale und entzündungsfördernde Zytokine aktiviert werden. Aktuelle Daten zeigen, dass die p38α Inhibition bei der Behandlung von Kolitis-assoziiertem Darmkrebs (CRC) großes Potential aufweist. Darmtumore, die mit einem Colitis Ulcerosa oder Morbus Crohn Hintergrund in Verbindung gebracht werden, machen jedoch nur einen kleinen Teil der Darmkrebs-Fälle aus.

Um das therapeutische Potential der p38α-Hemmung bei Kolitis-unabhängigem Darmkrebs zu untersuchen, habe ich CRC-Mausmodelle mit Hilfe von Organoiden generiert. Organoid Kulturen von murinen Kolonepithelzellen wurden *in vitro* durch genetische Modifikation von *Apc*, *Kras* und *Trp53* sowie unter Verwendung von CRISPR/Cas9 und *cre*-Rekombinase transformiert und etabliert. Nach der Transformation wurden diese Kulturen zurück in Mäuse transplantiert, in welchen sie histologisch eindeutig klassifizierbare kolorektale Tumore bildeten. Durch die Injektion von Organoidzellen in die Milz konnte eine Tumorbildung in der Leber induziert werden, welche eine Analyse von CRC-Metastasen möglich macht.

Mit Hilfe von shRNA-Interferenz konnte ich nachweisen, dass *Mapk14*/p38α einen potentiellen Kandidaten für die Behandlung des CRC darstellt. Die Behandlung von Darmtumoren mit spezifischen und gut etablierten p38α-Inhibitoren (Skepinone-L, PH797804) führte jedoch zu keinem ausgeprägten therapeutischen Effekt. Anhand mechanistischer Studien konnte gezeigt werden, dass eine erhöhte Aktivität der p38α-Kinase während der CRC Therapie mit den o.g. Inhibitoren einer vollständigen Hemmung des p38α-Signalweges entgegenwirkt.

Um eine vollständige Blockade des p38α Signalweges bei Darmkrebs zu ermöglichen, habe ich eine neuartige Klasse von Typ 1,5 p38α-Inhibitoren (generiert von der AG Laufer) mit pikomolarer Aktivität und signifikant verbesserter Targetresidenzzeit getestet. Ich habe diese Inhibitoren in verschiedenen CRC-Organoidkulturen analysiert und einen starken therapeutischen Effekt basierend auf einer Induktion von DNA-Schäden und eines veränderten G2 / M-Checkpoints beobachtet. Diese Typ 1,5 p38α-Inhibitoren wurden von Mäusen gut vertragen und zeigten *in vivo* großes Potential.

Um den therapeutischen Effekt dieser neuen Verbindungen in humanem CRCs zu bestimmen, habe ich Patienten basierte CRC-Organoidkulturen generiert. Diese Kulturen zeigten eine Resistenz gegen Standard Chemotherapien und gegen die etablierten p38α-Inhibitoren, reagierten jedoch stark auf eine Behandlung mit den p38α-Inhibitoren der neuen Generation.

Zusammengenommen zeigen meine Daten, dass p38α-Inhibitoren der neuen Generation mit optimierter Targetresidenzzeit ein großes therapeutisches Potential für die Behandlung von fortgeschrittenem Darmkrebs haben.

1. Introduction

1.1 Colorectal cancer

1.1.1 Epidemiology and risk factors

Colorectal cancer (CRC) represents a major health and socio-economic problem with nearly two million new cases in 2018. According to the GLOBOCAN 2018 CRC is the 2nd most commonly diagnosed cancer entity in women and the 3rd most in men worldwide, therefore accounting for approximately 10% of the annually diagnosed cancer cases and cancer-related deaths in both genders [1]. Since the risk of developing CRC increases with age the highest rates occur in countries with high Human Development Indices (HDIs) due to the augmented life expectancy. The median age at diagnosis in the US is 66 years in men and 72 years in women, tough a shift towards the diagnosis at a younger age has been observed since 1990 [2]. While incidence and mortality rates are slightly decreasing in developed countries due to early intervention programs, the western lifestyle increases the risk of the CRC development at a younger age. Risk factors include male sex, physical inactivity, obesity, smoking, high red meat and alcohol intake [3]. Besides environmental risk factors, there is a genetic predisposition towards developing CRC in individuals with a positive family history (1.9 to 4.4 fold increase) [4]. In a small subgroup of CRC patients the cause of the disease is a hereditary syndrome.

The classification into non-polyposis and polyposis syndromes is based on the amount and characterization of intestinal polyps. The hereditary non-polyposis CRC (HNPCC), also called Lynch syndrome, is caused by a genetic defect in the DNA mismatch repair (MMR) that results in tumors with microsatellite instability (MSI) [5]. Representative for the familial adenomatous polyposis (FAP) syndrome is the diagnosis of up to thousands adenomatous colorectal polyps arising already at a young age. A germline mutation in one of the most frequently mutated genes in CRC, the tumor suppressor adenomatous polyposis coli (*APC*), is the underlying cause of the disease [6]. Taken together hereditary non-polyposis and polyposis syndromes account for approximately 5 to 7% of all CRC cases [5].

1.1.2 Pathogenesis

The majority of colorectal tumors develop within several years from aberrant crypts to precancerous polyps and finally to CRC. 70 to 90% of all CRC cases show a progression according to the adenoma-to-carcinoma pathway which is correlated with sequential mutations in the *APC*, *RAS* or *RAF* and *TRP53* genes (Fig. 1). Those sporadic mutations lead to altered *WNT*, mitogen-activated kinase (MAPK) and *MYC* signaling. The less frequent serrated neoplasia pathway (10-20%) can be distinguished by CpG island methylation, an epigenetic mechanism to inactivate gene expression. CpG island methylation can either result in the outgrowth of microsatellite stable or instable tumors, depending on the affected gene. In the case of the DNA damage repair gene MutL homolog 1 (*MLH1)*, the methylation of the promotor region leads to MSI due to a deficiency of the DNA MMR [7, 8].

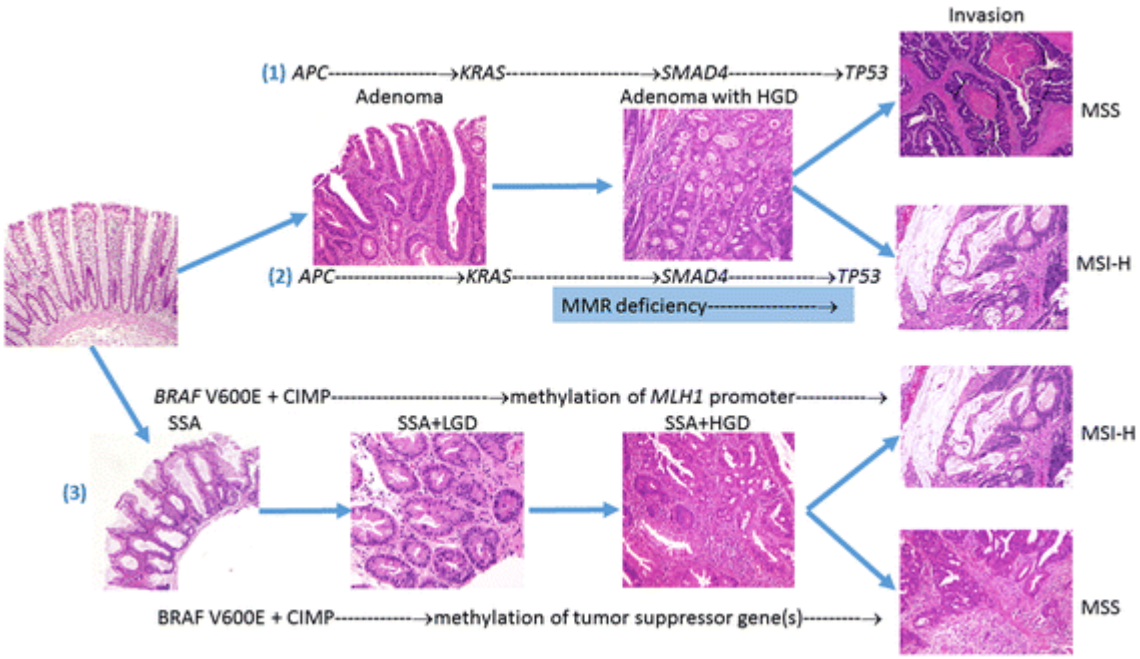

Figure 1. Overview of the three major pathways causing CRC (1) Adenoma-to-carcinoma pathway resulting in microsatellite stable (MSS) tumors via oncogene activation (*KRAS*) and tumor suppressor inactivation (*APC*, *SMAD4*, *TRP53*). **(2)** Lynch syndrome pathway leading to microsatellite instable (high MSI-MSI-H) tumors due to a deficiency in DNA MMR. **(3)** Serrated neoplasia pathway with characteristic CpG island methylation. Depending on the affected genes both MSS and MSI-H tumors can arise. HGD: high-grade dysplasia; LGD: low-grade dysplasia; SSA: sessile serrated adenoma. CIMP: CpG island methylator phenotype (adapted from Gonzales et al., 2017 [8]).

CRC cancer can also develop in a background of chronic inflammation, such as Colitis and inflammatory bowel disease (IBD). Colitis-associated cancer (CAC) represents only 1 to 2% of all CRC cases [9]. Chronic inflammation greatly influences the sequential mutagenesis of CRC progression. Whereas *TRP53* mutations occur late in the carcinogenesis of colitis independent CRC, it is an early event in the onset of CAC [10]. In CAC, the mutation of *TRP53* is linked to inflammation induced DNA damage, an irrelevant mechanism in the early stages of common CRC development. In contrast to the more prevalent CRC, which does not develop in the background of chronic inflammation, the loss of the tumor suppressor *APC* is a late incident in the CAC carcinogenesis [11].

Among all CRC subtypes activating *KRAS* mutations are found in 40% of all tumors. Constitutive active *BRAF* is a less frequent mutagenesis event (10%). Inactivating *PTEN* and activating phosphatidylinositol-4,5-bisphosphate 3-kinase catalytic subunit-α (*PIK3CA*) transformations occur in 30 and 20% of the patients, respectively. The WNT signaling pathway is most frequently affected by inactivating *APC* (70%) and in rare cases by activating *CTNNB1* (2%) mutations. The loss of *TRP53* function can be detected in 50% of all CRC cases. Other CRC-related mutations affect *SMAD*4 or the transforming growth factor-β receptor 2 (*TGFBR2*), as well as other components of the Mitogen-activated Protein Kinase (MAPK), PI3K and TGFβ signaling pathways [12].

1.1.3 Diagnosis and treatment options

The early detection and endoscopic removal of precancerous polyps have helped to decrease the CRC incidence in developed countries. Participating in CRC screening programs is a recommendation for individuals beginning at age 50 (World Gastroenterology Organization, WGO) in order to prevent CRC development and to intervene at a stage with a better prognostic outcome. Due to hesitancy towards the effective but invasive colonoscopy and the fact that CRC is a mostly asymptomatic disease in the less advanced stages, 21% of the US CRC patients are already diagnosed with tumors in an advanced or metastatic stage (according to the American Cancer Society). The five-year survival prognosis strongly differs between patients with local CRC (90%) and patients suffering from distant CRC metastasis (10%) [13].

During endoscopic screening, most adenomatous polyps can be resected directly, if necessary together with the underlying submucosa and analyzed via Immunohistochemistry (IHC) [14]. For further progressed tumors, laparoscopy of the primary disease and surgery of resectable metastases is the first choice to remove the cancerous tissue. Surgery can be combined with neoadjuvant radiotherapy and chemotherapy (fluoropyrimidines). Although preoperative treatment has been shown to reduce local recurrence, no beneficial effect on overall survival could be observed [15, 16]. Adjuvant fluoropyrimidine-based chemotherapy is only considered in high risk cases, e.g. when more than 12 lymph nodes were resected and positive resection margins are detected [17]. Nonetheless, not every patient can be considered for surgery, depending on the general fitness, the stage of the disease and the localization of primary tumor and metastases. Unresectable metastatic disease was commonly treated with combinatorial chemotherapy using leucovorin, 5-fluorouracil and either oxaliplatin (FOLFOX) or irinotecan (FOLFIRI). The FOLFOXIRI protocol takes advantage of all three chemotherapeutica and results in more effective tumor growth control, but also increased toxicity [18]. However, overall survival following first-line therapy with chemotherapeutic agents is only at 16 to 20 months [19].

Besides chemotherapy targeted therapy is widely used for the treatment of metastatic or unresectable CRC. Since an overexpression of the epidermal growth factor receptor (EGFR) can be found in approximately 80% of the cases, the EGFR-targeting monoclonal antibodies cetuximab and panitumumab have been considered for CRC therapy [20]. Although cetuximab and panitumumab lead to an increase in overall survival when combined with FOLFOX, they do not show any efficacy in tumors with activating *KRAS* or *NRAS* mutations [21]. Another therapeutic option is to disturb the vascular network of the tumor. The vascular endothelial growth factor A (VEGF-A) targeting monoclonal antibody bevacizumab directly interferes with tumor angiogenesis and improves the overall survival in combination with FOLFIRI [22]. Alongside bevacizumab the recombination fusion protein aflibercept has anti-angiogenic properties as well. The drug consists of the extracellular domains of the human VEGF receptor fused to the Fc receptor of human Immunoglobulin G (IgG) and prolongs the overall survival in combination with FOLFIRI [23]. Other targeted therapies include multi-kinase inhibitors for the blockade of MAPK signaling (among others erlotinib, sorafenib, vemurafenib) and immune checkpoint inhibitor therapy.

The latter represents a therapeutic strategy for tumors with high MSI that renders them more immunogenic than MSS CRC. However, this accounts only for 4% of all tumors. Furthermore, approximately half of the patients receiving immune checkpoint inhibitors do not respond to the treatment. This includes therapies targeting the programmed cell death-1 protein (PD-1, pembrolizumab, nivolumab) or cytotoxic T-lymphocyte associated protein 4 (CTLA-4, ipilimumab) [24, 25], highlighting the need for optimized CRC therapy.

Taken together, combinatorial therapies have led to an increase in progression-free survival (PFS) and life expectancy of CRC patients, however the 5 year survival rates for patients with advanced metastatic disease are still very low.

1.2 p38α inhibition in CRC

MAPK14 (p38α) is a serine-threonine protein kinase that is part of the MAPK signaling network. p38α belongs to the p38 Mitogen-activated protein kinase family which also includes p38β (*MAPK11*), p38γ (*MAPK12*) and p38δ (*MAPK13*). p38α is ubiquitously expressed and also p38β (*MAPK11*) was detected in a wide range of tissues, though at lower levels than p38α. The tissue specific expression of the kinases p38γ (*MAPK12*) and p38δ (*MAPK13*) can be linked to the skeletal muscle and endocrine glands, respectively [26, 27].

p38α plays an important role in the cellular stress response and in inflammatory signaling. Upon lipopolysaccharid (LPS) activation, p38α induces the synthesis of the inflammatory cytokines tumor-necrosis factor α (*TNFα*) and interleukin-1 (*IL-1*) [28]. However, the p38α pathway is activated by a variety of extracellular stimuli, including cytokines, growth factors, toxins, oxidative stress and nutrient availability. Signal transduction following p38α activation is mediated through phosphorylation of protein kinases (MAPK-activated protein kinase 2 - *MAPKAP-K2*), transcription factors (activating transcription factor 2 - *ATF2*, C/EBP homologous protein - *CHOP*, *TRP53*) and other cell regulatory proteins (heat shock protein 27 - *HSP27*, cell division cycle 25 - *CDC25*) [26]. Numerous processes are regulated through the extensive p38α network including inflammation, proliferation, differentiation, survival or cell-death.

In cancer, dual functions of p38α have been reported, depending on the stage of the disease. In a mouse model of colitis-induced colon cancer, the knockout of p38α resulted in increased tumorigenesis of the intestinal epithelium. In contrast, genetic knockout or pharmacological inhibition of p38α (using the p38α inhibitor PH797804) in already established murine CAC reduced the tumor burden [29]. Similar findings are reported for breast cancer mouse models, where increased p38α activity hindered tumor initiation [30] but the treatment with the p38α inhibitor AZ10164773 showed anti-proliferative properties in tumor-bearing mice [31]. Furthermore, p38α has been shown to control proliferation and cellular homeostasis in healthy tissue of the lung and liver highlighting its role as a tumor suppressor [32, 33]. However increased p38α expression correlates with a poor prognosis in many cancers supporting the tumor-promoting capacity and the dual role of this MAP kinase [34-38].

p38α also plays a role in resistance towards cancer therapies. In a mosaic mouse model of hepatocellular carcinoma (HCC) p38α was involved in the acquired resistance towards the multi-kinase inhibitor sorafenib. The therapeutic effect could be restored by combining sorafenib with Skepinone-L, a highly selective p38α inhibitor [39]. In CRC, pharmacological p38α inhibition via SB202190 sensitized irinotecan- or cisplatin-resistant human CRC cells towards the chemotherapy *in vitro* as well as in a xenograft mouse model [40, 41].

In clinical trials, p38α inhibitors were mainly used for the treatment of chronic inflammatory diseases, e.g. rheumatoid arthritis, since the kinase was first identified for its role in inflammatory signaling. Of note, recent studies also investigate the therapeutic potential of p38α inhibitors for the treatment of advanced and/or metastatic cancer including lymphoma (LY2228820, trial NCT01393990; LY3007113, trial NCT01463631) (clincicaltrials.gov). Taken together, p38α may not only represent a target for overcoming therapy resistance in CRC but could also be an Achilles heel for advanced colon tumors, which are relying on the stress kinase regarding tumor maintenance.

1.3 Organoid cultures and CRC research

In 2009, the Clevers laboratory published the generation and maintenance of three-dimensional (3D) organotypic colon tissue cultures, so called “mini-guts”. The first organoid cultures were established using leucine-rich-repeat-containing G-protein-coupled receptor 5 (Lgr5) positive stem-cells. These cells are located at the bottom of the intestinal crypt and harbor a nearly unlimited self-renewing potential. Paneth cells, enterocytes, goblet cells and enteroendocrine cells derive from the Lgr5 positive progenitors and build the crypt-villus-axis [42]. Taking advantage of known factors of the intestinal homeostasis, Sato et al. developed a specialized medium and embedded the isolated crypts in a scaffold matrix (Matrigel) in order to establish a physiological 3D culture. In line with the architecture of the intestinal epithelium, these organoids grew in budding structures with several villi and an enclosed lumen. Furthermore, Lgr5 positive stem-cells, paneth cells, enterocytes, goblet cells and enteroendocrine cells could be identified in the correct cellular hierarchy. Expression analysis after many passages revealed, that the transcriptome of these organoids was more or less identical to freshly isolated crypts, hence the organotypic culture represents a highly physiological long-term self-organizing system (Fig. 2) [43].

Figure 2. Murine small intestinal organoids. High-resolution bright field microscopic picture (left panel). Schematic illustration of the representative cell types. Apoptotic cells are shed into the lumen. CBC (crypt base columnar cells). Scale bar = 50 µm. Adapted from O’Rourke et al., 2016 [44].

In the following years, this culturing system was adapted for other organs and optimized for a variety of human tissues. Organoids were either isolated from adult stem cells (ASCs) or from induced pluripotent stem cells (iPSCs) and were able to

recapitulate their organ counterparts. Among others, organoid cultures of the lung [45], liver [46], pancreas [47], colon [48], stomach [49], prostate [50, 51], esophagus [52], mammary gland [53], kidney [54] and even the brain [55, 56] have been developed. Besides the usability of organoids to investigate tissue development and organization, the 3D tissue culture system harbors immense potential for translational cancer research. Patient-derived organoid biobanks are considered to be a new gold standard for drug screens and expression analysis. Such patient-derived organoids could be so far established from colon [48, 57], stomach [49], esophagus [48], pancreas [47, 58], liver [59], kidney [54, 60], bladder [61], ovarian [62] and breast cancer [53]. The analysis of a patient-derived CRC organoid biobank with over 50 samples revealed a broad range of mutational profiles fitting to the results of The Cancer Genome Atlas (TCGA) database. Furthermore, the maintenance of the histopathological features and heterogeneity of the original tumor could be proven *in vitro* and in organoid xenografts [63]. Such biobanks are considered to represent suitable tools for drug screens, drug development and personalized therapy. For example, in a study conducted by Verissimo et al. in 2016 a CRC organoid biobank was used to analyze therapy options in wildtype and *RAS* mutant organoids [64].

Alongside the possibilities regarding translational research also basic research profits from organoid applications. Since the cellular architecture of the corresponding organ is recaptured in organoid cultures, a more complex analysis of differentiation, gene function and cellular processes is achievable. For example, lung organoids are used for infectious disease studies [65], intestinal organoids are widely used to analyze barrier function against toxins or microbes [66]. Furthermore, organoids can be genetically modified in order to study tumorigenesis, therapy resistance or disease development. Persistent genetic manipulation can be achieved using the CRISPR/Cas9 system to generate specific mutations, knockouts or knockins [67]. Short hairpin RNA (shRNA) or small interfering RNA (siRNA) technology can be applied with adapted retroviral or lentiviral transduction protocols [68, 69], enabling the analysis of gene knockdown in organoid cultures. Since organoids represent more physiological cancer models than traditional monolayer cell cultures and are easily genetically modified, they can be seen as a missing link between biological *in vitro* and *in vivo* models [70].

1.4 Mouse models of CRC

Due to the fact that cancer organoids preserve the histopathological features of the originating tumor they present physiological tools for *in vivo* analysis when injected into mice [63]. Since the organoid technology was firstly developed in 2009, the use of organoid-based mouse models represents a rather novel CRC research tool.

CRC mouse models can be divided into three groups; chemically induced carcinogenesis models, genetically engineered mouse models (GEMMs) and tumor tissue or cell injection models. Chemically induced models are most commonly based on the administration of the carcinogens dextran sulfate sodium (DSS) and/or azoxymethane (AOM), which lead to the development of CAC [71, 72]. This enables the investigation of carcinogenesis induced by chronic inflammation; however CAC represents a subgroup of CRC, accounting for only 1 to 2% of all CRC cases [9]. In contrast to AOM and DSS induced carcinogenesis, GEMMs allow for CRC research in defined genetic backgrounds. The first GEMM for CRC was developed in 1990 by Moser et al. and termed multiple intestinal neoplasia (Min). The N-ethyl-N-nitrosourea (ENU) induced mutagenesis resulted in a loss of function mutation in the tumor suppressor *Apc* causing the development of multiple intestinal adenomas [73]. Although Apc^{Min} mice predominantly develop polyps in the small intestine that rarely progress to carcinomas the model was commonly used for functional genetic, tumorigenesis, treatment and prevention studies [74]. In the following years many GEMMs were generated based on known CRC driver mutations with the goal to establish advanced CRC and metastatic disease. The utilization of the Cre-loxP system allowed for tissue specific gene silencing by recombination of loxP flanked exon regions or oncogene activation by removing floxed Stop codons of transgenes [75]. Temporal control of mutagenesis was achieved by fusing the Cre-recombinase to the estrogen receptor, thereby creating the possibility to start the carcinogenesis in adult animals via tamoxifen administration [76]. One of the major drawbacks of those early GEMMs was the limited metastases formation in less aggressive genotypes. Until the generation of GEMMs with multiple mutations in oncogenes and tumor suppressors metastases formation in the liver was infrequent [74], although distant liver metastases develop in approximately 25% of the patients within 5 years following diagnosis [77]. However, the generation of GEMMs and breeding of the

desired genotype is not only time consuming but also an inflexible tool for the analysis of multiple genetic alterations.

The transplantation of patient-derived tumor tissue and human CRC cell lines enables the rapid generation of cancer bearing mice with distinct mutational profiles. For the generation of so called xenografts immune-deficient mice have to be used in order to avoid rejection. Unfortunately, the success of engraftment is limited and upon subcutaneous injection no metastases formation can be observed [78, 79]. Orthotopic transplantations into the intestinal serosa lead to tumor development in a more physiological microenvironment compared to subcutaneous tumors; metastases formation in the lung and the liver can be mimicked with cancer cell injections into the tail vein or the spleen [78, 80]. Using patient-derived tumor xenogafts (PDTXs) or patient-derived tumor organoids (PDTOs) in xenograft models offers the advantage that histopathological features of the primary tumor are preserved [81]. Since organoid cultures can be established from a variety of tumor tissues the system provides more flexibility than the transplantation of patient-derived tumor pieces (PDTXs). Furthermore, in contrast to traditional 2D cell lines, organoids were demonstrated to be genetically stable in culture, hence the tumor heterogeneity is maintained [57, 58, 82]. In contrast to xenograft models, the generation of murine allografts enables tumor development in mice with a functional immune system, thereby allowing for more complex systemic studies. Before injection, cell lines as well as organoids can be transformed *in vitro* in order to investigate specific mutations allowing for an immense genetic flexibility. In the recent years several laboratories used organoid cultures for orthotopic transplantations and created highly physiological tumor models with great translational potential. For example, O'Rourke et al. established a protocol for the transplantation of engineered organoids into the colon of mice and were able to induce primary tumors in the colon as well as metastatic disease. They were also able to mimic metastasis formation in the lung or the liver via intravenous or splenic injection [83]. Another interesting mouse model represents the transplantation of cerebral organoids into the cortex of mice [84]. In conclusion, both human and murine organoid cultures are highly physiological tools that offer great research potential *in vitro* and *in vivo*.

1.5 Aim of the study

Despite the steady progress in targeted therapies, CRC remains a disease with poor survival prognosis. Since immunotherapies are mostly not effective in these tumor type, more efficient targeted therapies are urgently needed. The stress kinase p38α was found to be beneficial for CRC maintenance and it was shown that genetic ablation of the p38α gene *Mapk14* inhibits colitis-induced colorectal cancer [29]. However, colitis-induced colorectal tumors represent only a small fraction of human CRC.

Taking advantage of complex tissue culture methods, and organoid-based CRC mouse models, I aimed to analyze the role of p38α in colitis-independent CRC and to investigate the therapeutic value of p38α inhibition in these tumors.

2. Material and Methods

2.1 Material

2.1.1 Chemicals

If not mentioned otherwise, all chemicals and solutions used in this study were purchased from the following companies: AppliChem, Biosciences, Carl Roth, Corning, Fermentas, Fluka, GE Healthcare, Invitrogen, Invivogen, Life Technologies, Merck, Millipore, Peprotech, Promega, Peqlab, R&D Systems, Sarstedt, Serva, Selleckchem, Sigma Aldrich, Thermo Fisher, TOCRIS, Vectorlabs or VWR.

2.1.2. Enzymes

Restriction enzymes, Alkaline Phosphatase Calf Intestinal (CIP), DNaseI, T4 DNA ligase were purchased from NEB (New England Biolabs). The supplier of Platinum Pfx DNA Polymerase was Invitrogen. GoTaq®Green Master Mix was purchased from Promega.

2.1.3 Kits

Table 1: Kits used in this study, including company

Kit	Company
AllPrep DNA+RNA Mini Kit	Qiagen
CellTiter-Glo® 2.0	Promega
DAB solution	Zytomed
DC-Protein Assay	Bio-Rad
GoTaq® genotype Kit	Promega
Molecular Probes™ Click-iT™ EdU Alexa Fluor™ 555 Bildgebungs-Kit	Thermo Fisher
Plasmid Maxi Kit	Qiagen
PrimeScript RT Master Mix	Takara Clontech
Qiaquick Gel Extraction Kit	Qiagen
Surveyor® Mutation Detection Kit for Standard Gel	IDT

Electrophoresis	
SYBR Premix Ex Taq (Tli RNase H Plus)	Takara Clontech
TNF alpha Mouse Uncoated ELISA Kit	Thermo Fisher

2.1.4 Buffers and solutions

Table 2: buffers and solutions used in this study, including composition

buffer/solution	composition
Anaesthesia	2 ml Ketamin (50 mg/ml), 500 µl Xylazin (20 mg/ml), ad 10 ml 0.9% NaCl
Chelating buffer	2 mM EDTA, pH8, in DPBS
DNA loading buffer (5x)	0.25 % orange G, 15 % (w/v) Ficoll type 400
Eosin solution	0.5 % Eosin, 0.002 % $C_2H_4O_2$
HBS (2x)	1.5 mM Na_2HPO_4 (pH 7.0), 280 M NaCl, 50 mM HEPES, 12 mM Dextrose, 10 mM KCl (best out of pH 6.96; 7.00; 7.04; 7.08)
NP40 lysis buffer	50 mM TrisHCl (pH 7.5), 150 mM NaCl, 0.5 % NP-40, 1x Complete mini® (Roche, Basel, Schweiz)
PBS (10 x)	100 mM $Na_2HPO_4x2H_2O$, 20 mM KH_2PO_4, 1.37 M NaCl, 27 mM KCl (pH 7.4)
PBST	0.1 % Tween 20 in PBS
Permeabilization and blocking buffer	5% BSA, 0.2% Triton X-100,0.1% Tween 20 in TBS
PFA in PBS	4 % PFA in PBS (pH 7.4)
PFA in TBS	4 % PFA in TBS (pH 7.4)
Protein-loading buffer, Laemmli (4x)	200 mM Tris/HCl (pH 6.8), 8 % SDS, 20 mM DTT, 40 % glycerol, 0.33 % bromphenolblue
SDS-running buffer (10x)	250 mM Tris Base, 1.92 M glycine, 1 % SDS
Sodium citrate buffer	10 mM $C_6H_5Na_3O_7$ (pH 6.0)
TAE (50 x)	2 M Tris Base (pH 8.5), 1 M glacial acetic acid, 50 mM EDTA
TBS (10x)	500 mM Tris.HCl, (pH 7.4), 1500 mM NaCl
TBST	0.1 % Tween 20 in TBS
Transfer buffer	48 mM Tris-HCl (pH 8.3), 39 mM glycine, 20 % methanol, 0.037 % SDS

2.1.5 Antibodies

Table 3: antibodies used in this study

Primary antibodies						
ID	antigen	species	application	dilution	company	conjugation
242	ATF-2	mouse	WB	1:200	Santa Cruz	
8398	ATF2 (Thr71)	mouse	WB	1:200	Santa Cruz	
4539	cdc2 (Tyr15)	rabbit	WB	1:1000	CST	
76541	CDX2	rabbit	IF/IHC	1:500	abcam	
97511	CK20	rabbit	IF	1:100	abcam	
9661	Cl. Caspase-3 (Asp175)	rabbit	WB	1:1000	CST	
4138	Cyclin B1	rabbit	WB	1:1000	CST	
9718	Histone H2A.X (Ser139)	rabbit	WB	1:1000	CST	
2401	HSP27 (Ser82)	rabbit	WB	1:1000	CST	
2406	HSP27 (Ser82)	rabbit	WB	1:1000	CST	
3042	MAPKAPK-2	rabbit	WB	1:1000	CST	
3007	MAPKAPK-2 (Thr334)	rabbit	WB	1:1000	CST	
4511	p38 MAPK (Thr180/Tyr182)	rabbit	WB	1:1000	CST	
9218	p38α MAPK	rabbit	WB	1:1000	CST	
nbp2-19662	p38α MAPK	rabbit	IF	1:100	Novus Bio	
81714	Pan-CK	mouse	IHC	1:50		
9251	SAPK/JNK (Thr183/Tyr185)	rabbit	WB	1:1000	CST	
V9131	vinculin	mouse	WB	1:10000	Sigma Aldrich	
2125	α-tubulin	rabbit	WB	1:1000	CST	
5316	β-actin	mouse	WB	1:1000	Sigma Aldrich	

Secondary antibodies

ID	antigen	species	application	dilution	company	conjugation
TP-015-HD	anti-polyvalent	goat	IHC	x	Thermo Scientific	biotin
115-035-062	mouse	goat	WB	1:5000	Dianova	HRP
A-11029	Mouse	goat	IF	1:1000	Invitrogen	Alexa 488
111-035-045	rabbit	goat	WB	1:5000	Dianova	HRP
A-11034	Rabbit	goat	IF	1:1000	Invitrogen	Alexa 488
A-11037	Rabbit	goat	IF	1:1000	Invitrogen	Alexa 594

2.1.6 Oligonucleotides

All oligonucleotides used in this study are listed in table 4. Oligonucleotides were obtained from MWG, Sigma or Cold Spring Harbor laboratories (Scott Lowe Laboratory). Cloning and sequencing primer were designed with SnapGene Viewer. qRT-PCR primer were designed with the primer designing tool from NCBI. Genotyping primer sequences were obtained from the Jackson Laboratory website.

Table 4: Oligonucleotides used in this study

genotyping	
primer	sequence
Kras LSL 1	GTCTTTCCCCAGCAGAGTGC
Kras LSL 2	CTCTTGCCTACGCCACCAGCTC
Kras LSL 3	AGCTAGCCACCATGGCTTGAGTAAGTCTGCA
p53 loxP recombined	GAAGACAGAAAAGGGGAGGG
p53 loxP A WT	CACAAAAACAGGTTAAACCCAG
p53 loxP B lox	AGCACATAGGAGGCAGAGAC

surveyor	
primer	sequence
pX330.Apc.2 fw	CAGCACTTGAAATCTCACAGCTTGAC
pX330.Apc.2 rev	GAAGAAGAGCTGGGCAATACCGTAG

qRT-PCR

primer	sequence
Mapk14 qPCR	GCATCGTGTGGCAGTTAAGA (fw)
mouse II	GTCCTTTTGGCGTGAATGAT (rev)
TNFa murine	TACTGAACTTCGGGGTGATTGGTCC (fw)
	CAGCCTTGTCCCTTGAAGAGAACC (rev)
STAT3 qPCR	CAACGACCTGCAGCAATACC (fw)
mouse	GTAGCACACTCCGAGGTCAG (rev)
IL6 qPCR mouse	GCCAGAGTCCTTCAGAGAGAT (fw)
	GGAGAGCATTGGAAATTGGGGT (rev)
β-actin	GCCACTGTCGAGTCGCGT (fw)
	GATACCTCTCTTGCTCTGGGC (rev)
qPCR Ikbα	AAATCTCCAGATGCTACCCGAGAG (fw)
	ATAATGTCAGACGCTGGCCTCCAA (rev)

cloning

primer	sequence
miR-E EcoRI_rev	TTAGATGAATTCTAGCCCCTTGAAGTCCGAGGCAGTAGGCA
miR XhoI_for	CAGAAGGCTCGAGAAGGTATATTGCTGTTGACAGTGAGCG

sequencing

primer	sequence
pCaggs seq fw	CGGCTCTAGAGCCTCTGCTAACCATGT
MIR30fw	TGTTTGAATGAGGCTTCAGTAC

sgRNAs

sgRNA	sequence
pX330.Apc.2	GTCTGCCATCCCTTCACGTT

shRNAs

shRNA	sequence
Ren.713	TGCTGTTGACAGTGAGCGCAGGAATTATAATGCTTATCTATAGTGAAG
	CCACAGATGTATAGATAAGCATTATAATTCCTATGCCTACTGCCTCGGA
Mapk14.1416	TGCTGTTGACAGTGAGCGCCAGGTATGTTCAAAACTGTCATAGTGAAGC
	CACAGATGTATGACAGTTTTGAACATACCTGTTGCCTACTGCCTCGGA

Mapk14.168	TGCTGTTGACAGTGAGCGAAAGGTCACTGGAGGAATTCAATAGTGAAG CCACAGATGTATTGAATTCCTCCAGTGACCTTGTGCCTACTGCCTCGGA
Mapk14.2131	TGCTGTTGACAGTGAGCGAAAAAGGGTTGTTAGACACAAATAGTGAAG CCACAGATGTATTTGTGTCTAACAACCCTTTTGTGCCTACTGCCTCGGA
Mapk14.2486	TGCTGTTGACAGTGAGCGCCAGGTCTTGTGTTTAGGTCAATAGTGAAG CCACAGATGTATTGACCTAAACACAAGACCTGTTGCCTACTGCCTCGGA
Mapk14.2605	TGCTGTTGACAGTGAGCGCCCACCTCAGTGTGCAGTTCAATAGTGAAG CCACAGATGTATTGAACTGCACACTGAGGTGGTTGCCTACTGCCTCGGA
Mapk14.2948	TGCTGTTGACAGTGAGCGCAAGCCTAGTTTTCAAATTCAATAGTGAAG CCACAGATGTATTGAATTTGAAAACTAGGCTTTTGCCTACTGCCTCGGA

The shRNA sequences were designed as 21 nucleotide RNAs and were provided by Johannes Zuber. These sequences were embedded into 97mer oligonucleotides that form stem loop stem structures.

2.1.7 Plasmids

For the transduction of cells the all in one retroviral plasmid TRE(3G) GFP miR-E PGK Puro IRES rtTA3 (RT3GEPIR) was used, which was kindly provided by Johannes Zuber. The plasmid encoding Cas9n and a sgRNA targeting *Apc* (pX330.Apc.2) was kindly provided by Wen Xue.

Mapk14 and Ren shRNA constructs were generated via PCR amplification of shRNA oligonucleotides (table 4) inserting EcoRI and XhoI restriction sites. The PCR products were cloned into RT3GEPIR.

2.1.8 Bacteria

The Subcloning Efficiency™ DH5α™ Competent Cells from Invitrogen were used for plasmid production via transfection and overnight cultures.

2.1.9 Cell lines

For the generation of viral particles the genetically modified human embryonic kidney cell line (HEK293T) Phoenix-ECO (ATCC® CRL-3214™) was used.

The human colorectal cancer cell lines HCT-15 (ATCC® CCL-225), HT-29 (ATCC® HTB-38) and HCT 116 (ATCC® CCL-247) were kindly provided by Klaus Schulze-Osthoff.

The murine colorectal cancer cell line *Kras*$^{G12D/+}$ x *Apc*$^{mut/+}$ x *Trp53*$^{-/-}$ (KAP) was generated from KAP organoids (see 2.3.5).

2.1.10 Organoid cultures

Murine organoids were generated from the colon of *Apc*$^{fl/fl}$ (C57BL/6-*Apc*^{tm1Tyj}/J) and *Kras*^{LSL} x *Trp53*$^{fl/fl}$ (B6.129-*Kras*^{tm4Tyj} *Trp53*^{tm1Brn}/J) mice.

The murine colorectal cancer organoid cultures *Kras*$^{G12D/+}$ x *Myc*^{OE} x *Trp53*$^{-/-}$ (KMP) and *Braf*^{V600E} x *Apc*$^{-/-}$ x *Trp53*$^{mut/mut}$ (BAP), based on previously established *Kras*^{LSL} x *Trp53*$^{fl/fl}$ and *Apc*$^{fl/fl}$ organoid cultures, were generated together with Agata Dylawerska.

Human colorectal cancer organoids were isolated from patient material (primary tumor or ascites material). All samples used for organoid culture establishment and biological analyses were obtained from the University Hospital of Tuebingen with written informed consent.

2.1.11 Mouse strains

The mouse strains used in this study were purchased from the Jackson Laboratory and bred in the animal husbandry at Morgenstelle, University of Tuebingen.

Table 5: mouse strains used in this study

name	mouse strain
Wildtype (WT)	C57BL/6
Apc$^{fl/fl}$	C57BL/6-*Apc*^{tm1Tyj}/J
Kras^{LSL} x *Trp53*$^{fl/fl}$	B6.129-*Kras*^{tm4Tyj} *Trp53*^{tm1Brn}/J
Trp53$^{fl/fl}$	B6.129P2-Trp53tm1Brn/J

2.2 Cell culture

All cell cultures were incubated at 37°C and 7.5% CO_2.

2.2.3 Media

Roswell Park Memorial Institute (RPMI) 1640 medium (Gibco) supplemented with 10% FCS and 1% Pencillin/Streptomycin was used for organoid-derived cell cultures. Human colorectal cancer cell lines were cultured in Dulbecco's Modified Eagle Medium (DMEM) medium (Gibco) enriched with 10% FCS, 1 mM sodium pyruvate, 0.1 mM Non-Essential Amino Acids Solution and 1x Penicillin/Streptomycin. Cells were frozen in DMEM or RPMI medium containing 20% FCS and 10% DMSO.

Additional substances e.g. for selection of RT3GEPIR containing cells, transduction or infection of cells, were used in the following concentrations:

Table 6: substances used in cell culture

Substance	Stock concentration	Final concentration
Chloroquine	10 mg/ml	2.5 µg/ml
Doxycycline	10 mg/ml	5 µg/ml
Polybrene	10 mg/ml	5 µg/ml
Puromycin	12.5 mg/ml	7.5 µg/ml

2.2.4 Transfection

Phoenix-ECO cells were transfected in order to produce retroviral particles for the stable transduction of cells. When Phoenix-ECO cells had reached 70% confluency the cells were treated with chloroquine for 30 min at 37°C. Following the chloroquine pre-treatment 20 µg of plasmid-DNA was mixed with 62.5 µl 2 M $CaCl_2$ and filled up with ddH_2O to a final volume of 500 µl. The plasmid solution was then slowly transferred (pipetting single drops) into a 15 ml falcon containing 500 µl of 2x HBS buffer while constantly bubbling air into the buffer. The plasmid-buffer mixture was incubated for 5 mins at RT and dropwise added to the cells. After 8 hours incubation the medium was refreshed. Retroviral particles were harvested after 24 additional hours and filtered through a 0.45 µm filter.

2.2.5 Stable transduction of cells

At 30% confluency target cells were used for transduction. Before the supernatant containing retroviral particles was added the cells were pre-treated with polybrene for 15 mins at 37°C. 100 µl of viral supernatant was added and distributed evenly over the cell surface. The transduction with 100 µl supernatant was repeated after 8 hours. After 24 hours of incubation, transduced cells were selected with two 24 hour cycles of puromycin.

2.3 Organoid culture

All organoid cultures were incubated at 37°C and 7.5% CO2.

2.3.3 Media

Table 7: media used for organoid culture

Splitting medium			
substance	Stock concentration	Final concentration	company
Gibco™ Advanced DMEM/F-12	1x	1x	Thermo Fisher
GlutaMAX	100x	1x	Thermo Fisher
HEPES	1 M	10 mM	Thermo Fisher
Primocin™	50 mg/ml	125 µg/ml	Invivogen

murine colon medium			
substance	Stock concentration	Final concentration	
Splitting medium	1x	1x	
B-27® Supplement	50x	1x	Thermo Fisher
N-2 Supplement	100x	1x	Thermo Fisher
Nicotinamide	1 M	10 mM	Sigma Aldrich
N-Acetyl-L-cysteine	500 mM	1.25 mM	Sigma Aldrich
Recombinant Murine Noggin	100 µg/ml	100 ng/ml	Peprotech
Recombinant Human R-Spondin-1	500 µg/ml	500 ng/ml	Peprotech

EGF Recombinant Mouse Protein	500 µg/ml	50 ng/ml	Thermo Fisher
Recombinant Human Wnt-3a Protein	100 µg/ml	100 ng/ml	R&D Systems

murine CRC medium

substance	Stock concentration	Final concentration	
Splitting medium	1x	1x	
B-27® Supplement	50x	1x	Thermo Fisher
N-2 Supplement	100x	1x	Thermo Fisher
Nicotinamide	1 M	10 mM	Sigma Aldrich
N-Acetyl-L-cysteine	500 mM	1.25 mM	Sigma Aldrich
Recombinant Murine Noggin	100 µg/ml	100 ng/ml	Peprotech

Human CRC medium

substance	Stock concentration	Final concentration	
Splitting medium	1x	1x	
B-27® Supplement	50x	1x	Thermo Fisher
N-2 Supplement	100x	1x	Thermo Fisher
Nicotinamide	1 M	10 mM	Sigma Aldrich
N-Acetyl-L-cysteine	500 mM	1.25 mM	Sigma Aldrich
Recombinant Murine Noggin	100 µg/ml	100 ng/ml	Peprotech
Recombinant Human R-Spondin-1	500 µg/ml	500 ng/ml	Peprotech
Animal-Free Recombinant Human EGF	50 µg/ml	50 ng/ml	Peprotech
Recombinant Human Wnt-3a Protein	100 µg/ml	100 ng/ml	R&D Systems
A83-01	0,5 mM	0,5 µM	TOCRIS
GastrinI	10 µM	10 nM	TOCRIS
SB202190	10 mM	2.5 µM	selleckchem
PGE2	1 mM	1 µM	R&D Systems

tumor digestion medium

Splitting medium	1x	1x	

Collagenase II	2,5 mg/ml	Thermo Fisher
Collagenase IX	2,5 mg/ml	Sigma Aldrich
Dispase II	1mg/ml	Sigma Aldrich

2.3.4 Isolation of murine colon organoids

Murine colon organoids were isolated from *Kras*^{LSL} x *Trp53*$^{fl/fl}$ and *Apc*$^{fl/fl}$ mice as described before [43]. In brief, dissected murine colons were flushed with ice-cold PBS and cut into small pieces. The colon fragments were washed several times with ice-cold PBS until the supernatant remained clear and free of debris. Afterwards the tissue was transferred to 2 mM EDTA chelating buffer and incubated for 30 mins at 4°C on an orbital shaker. Next, the supernatant was removed and the tissue fragments were vigorously resuspended in splitting medium containing 10% FCS. For crypt isolation tissue fragments were allowed to settle down by gravity and the supernatant was analyzed by inverted microscopy. Supernatants lacking crypts or containing too much debris were discarded and resuspension was repeated until the suspension was enriched for crypts. Supernatants containing crypts were centrifuged at 150 g for 5 mins. Colonic crypts were counted and embedded in 50 µl domes of Growth Factor Reduced (GFR) Matrigel^{TM} (Corning) and plated in 24-well plates (approximately 250-500 crypts per well). Following polymerization for 10 mins at 37°C Matrigel^{TM} (Corning) domes were overlaid with murine colon medium. For the first three days after isolation 10.5 µM Y-27632 dihydrochloride (Invitrogen) was added to the culture. The medium was refreshed every two to three days.

2.3.5 Patient derived organoid cultures

Human CRC organoids were either isolated from primary tumors (hCRC3, hCRC7) or ascites material (hCRC5) of patients. All patients gave their informed consent according to German law.

Upon arrival primary tumor material was washed twice in ice-cold splitting medium and cut into 2-4 mm pieces. Afterwards the tissue was transferred into tumor digestion medium supplemented with 100 µg/ml DNaseI and 10.5 µM Y-27632 dihydrochloride (Invitrogen). Tumor digestion was performed at 37°C on a shaker with 75 rpm rotation until 90% of the tissue was digested into single cells. The

digestion was stopped by adding the same amount of splitting medium. The mixture was centrifuged for 5 mins at 300 g. To perform red blood cell lysis the pellet was transferred into ACK lysing buffer (Thermo Fisher) for 5 mins at RT. ACK lysing buffer (Thermo Fisher) was removed by centrifugation for 5 mins at 300 g. Afterwards the pellet was resuspended in splitting medium and cells were counted using a Neubauer chamber. Following the final centrifugation for 5 mins at 300 g the cells were adjusted to roughly 1000 cells in 50 µl Growth Factor Reduced (GFR) Matrigel^{TM} (Corning) and plated in pre-warmed 24-well plates.

The ascites material was pelleted by centrifugation at 300 g and washed several times with ice-cold PBS before embedding the cells in domes of Matrigel^{TM} (Corning).

Within the first week of culture the human CRC medium was supplemented with 10.5 µM Y-27632 dihydrochloride (Invitrogen). The medium was refreshed every two to three days.

2.3.6 Splitting and single cell dissociation of organoids

Confluent organoids were split by mechanical dissociation into smaller cell clumps and re-plated in Matrigel^{TM} (Corning) domes. Depending on the organoid culture the splitting ratio was 1:2 to 1:6 once or twice per week.

For single cell isolation organoids were mechanically dissociated by pipetting and digested using TrypLE supplemented with 100 µg/ml DNaseI and 10.5 µM Y-27632 dihydrochloride (Invitrogen). The digestion was performed for 5 to 15 mins at 37°C.

2.3.7 Lipofectamine® transfection of murine colon organoids

Before transfection *Kras*^{LSL} x *Trp53*$^{fl/fl}$ organoids were mechanically dissociated by pipetting and digested into single cells using TrypLE supplemented with 100 µg/ml DNaseI and 10.5 µM Y-27632 dihydrochloride (Invitrogen). The digestion was performed for 5 to 15 mins at 37°C. After digestion, cells were resuspended in 450 µl murine colon medium supplemented with 10.5 µM Y-27632 dihydrochloride (Invitrogen) and plated in 24-well plates. Lipofectamine® 2000 (Invitrogen) transfection was performed according to the manufacturers' protocol. 1.5 µg of *cre*-recombinase and pX330.Apc.2 encoding plasmid DNA each were added to 50 µl Opti-MEM® medium and incubated with 50 µl Opti-MEM® medium supplemented

with 4 µl Lipofectamine® 2000 (Invitrogen) for 5 mins at RT. Next, the Lipofectamine® 2000 (Invitrogen) -plasmid solution was added to the dissociated organoids. After 6 hours of incubation at 37°C organoids were plated in Matrigel™ (Corning) and cultured with murine colon medium supplemented with 10.5 µM Y-27632 dihydrochloride (Invitrogen) [67]. Selection of transfected organoids was perfomed by the withdrawal of recombinant R-Spondin-1, EGF and Wnt-3a.

2.3.8 Retroviral infection of organoids

KAP 3D organoids were digested into single cells as described in 2.3.7 and transferred to a 5 ml low binding tube. 500 µl of viral supernatant (see 2.2.4) containing retroviral particles and polybrene were added to the cultures and incubated for 6 hours. Subsequently, the cultures were plated into Matrigel. After 48 hours of incubation, infected organoids were selected with three 24-hour cycles of puromycin.

2.4 Histological methods

2.4.3 Hematoxylin/eosin (H&E) staining

First tissue samples were fixed with 4% paraformaldehyde for 24 hours at RT. The fixed samples were then embedded in paraffin. 4 µm thick slices were cut using a microtome and dried afterwards at 65°C for 15 to 20 mins. To rehydrate the tissue the slides were incubated in xylol, xylol/ ethanol (1:1), 90% ethanol, 70% ethanol, 50% ethanol and water for 3 mins each.

The samples were incubated for 8 mins in hematoxylin (Gil II) to proceed with H&E staining. Following hematoxylin incubation, the slices were rinsed shortly with tap water and developed under running tap water for 10 mins. Afterwards they were incubated in eosin Y solution for 3 minutes, washed twice with MiliQ water and dehydrated via incubation in 90% ethanol, 70% ethanol, xylol/ ethanol (1:1) and xylol for 3 mins each. Samples were mounted with NeoMount and covered with a glass slide for long-term fixation and storage.

2.4.4 Immunohistochemistry staining (IHC)

For IHC tissue samples were processed as described for H&E staining. Following rehydration an antigen retrieval with boiling sodium citrate buffer (10 mM, pH 6.0, 0.5% Tween-20) was performed (15 to 20 mins). 5 mins incubation in 3% H_2O_2 was used to saturate endogenous oxidase activity. The samples were circled with a PAP pen and blocked with blocking solution (Zytomed) or 5% BSA for 5 mins at RT. The incubation with the primary antibody was performed over night at 4°C. The next day, the slides were washed with TBST and incubated with the secondary antibody for 1 hour at RT. After the incubation slides were washed once in TBST and biotin-HRP solution (1:300, Dako) was added for 15 mins. Before developing samples were washed twice in TBST. DAB developing solution (Zytomed) was added until a specific signal was observed under the microscope. The reaction was stopped via adding MiliQ water. Samples were counterstained with hematoxylin only and mounted as described before.

2.4.5 Immunofluorescence staining (IF) on cells and organoids

For IF cells and organoids were plated on Tissue Culture Chambers (Sarstedt). Organoids were plated in a mixture of Matrigel™ (Corning) and corresponding medium (1:10). Before fixation cells and organoids were allowed to attach for 24 hours. Then cells or organoids were fixed with 4% PFA at 4°C for 10 mins, washed with TBST and permeabilized with permeabilization and blocking buffer for 30 mins at RT on a shaker. For the p38α antibody from Novus Bio an additional 20 mins permeabilization step in ice cold Methanol was performed. After permeabilization the chambers were washed three times with TBST and the samples were incubated with primary antibody in 1% BSA in TBST over night at 4°C on a shaker. The next day samples were washed three times in TBST and incubated with fluorescent dye-labelled secondary antibody in 1% BSA in TBST for 60 mins at RT on a shaker. To remove the secondary antibody chambers were washed three times with TBST and mounted with VECTASHIELD HardSet mounting medium with DAPI (Vector Labs).

2.4.6 EdU proliferation assay

The Molecular Probes™ Click-iT™ EdU Alexa Fluor™ 555 Kit was used to analyze cell proliferation. Cells were plated on Tissue Culture Chambers (Sarstedt) and allowed to attach for 24 hours. Before starting the drug treatment in EdU supplemented medium the cells were synchronized by FBS withdrawal for 24 hours. After 24 hours of drug treatment and EdU incorporation cells stained according to the manufacturers' instructions.

2.4.7 Microscopic pictures and staining analyses

Microscopic pictures were taken with the Olympus BX63 (Olympus). Evaluation of antibody stainings was done by analyzing 10 to 20 optical fields using ImageJ.

2.5 Molecular biology techniques

2.5.3 Plasmid preparation from bacterial cultures

Bacteria were cultured using lysogenic broth (LB) medium consisting of 10 g/l bacto-tryptone, 5 g/l bacto-yeast extract and 20 mM NaCl (pH 7.5). LB based plates were made by adding 15 g/l agar. For selection of successfully transformed clones 50 µg/ml ampicillin was added.

For high yield preparation 350 ml LB-medium was inoculated with the respective bacteria and incubated over night at 37°C under constant shaking (170 rpm). The MaxiPrep Kit from Qiagen was used according to the protocol to extract plasmid DNA.

For low yield preparation 8 ml bacterial culture was used. Following overnight incubation as described before the bacterial culture was pelleted via centrifugation at 2000 rpm for 5 mins. The pellet was resuspended in 200 µl buffer P1. 200 µl buffer P2 was added and incubated for 5 mins to achieve cell lysis. Neutralization was performed by adding 200 µl buffer P3. The solution was carefully inverted five times and cell debris was pelleted via centrifuging at 13300 rpm for 10 mins. To precipitate DNA 400 µl isopropanol was added to 500 µl supernatant. The samples were centrifuged at 13300 rpm for 15 mins, the supernatant was discarded and the pellet

was washed with 70% ethanol at 13300 rpm for 5 mins. The pellet was air-dried and re-suspended in 30 µl ddH_2O.

2.5.4 Digestion of specific DNA fragments with restriction enzymes

10 µg of plasmid DNA or PCR products were digested with 0.5 µl of enzyme and the respective buffer (NEB) for at least 2 hours at 37°C in a volume of 20 µl. If size separation was necessary the reaction was loaded on an agarose gel. After cutting the band from the gel the DNA was purified with the QIAquick Gel Extraction Kit (Qiagen) according to the manufacturers' protocol.

2.5.5 Agarose gel electrophoresis

Depending on the DNA fragment size gels of 1% to 2% agarose and around 0.01% EtBr in 1x TAE buffer were poured. The DNA was separated at 130 V in 1 x TAE buffer. To determine band size the 100 bp or 1kb bechtop DNA ladders (Promega) were used. The agarose gel was visualized using UV light.

2.5.6 Dephosphorylation of DNA fragments

Backbone dephosphorylation was achieved by using 1 µl Calf Intestinal Phosphatase (CIP, NEB) in a total volume of 20 µl. The reaction was performed for 1.5 hours at 37°C:

2.5.7 Ligation of DNA fragments

0.5µl T4-ligase (NEB) was used for the ligation of backbone and insert. The reaction was performed over night at 4°C in a total volume of 10 µl.

Backbone to insert ratio was calculated according to the following formula: $amount(insert) = \frac{bp(Insert)}{bp(vector)} * 6 * 100\ ng$.

2.5.8 DNA purification

To maintain optimal conditions while cloning PCR products and DNA following restriction enzyme digestion or dephosphorylation were purified with the QIAquick Gel Extraction Kit (Qiagen).

2.5.9 Transformation of bacteria

5 µl freshly ligated plasmid solution was mixed with 40 µl Subcloning Efficiency™ DH5α™ Competent Cells cells. For successful transformation the mixture was incubated on ice for 30 mins, followed by a 20 second heat shock at 42°C. After the final incubation on ice for 2 mins the bacteria were plated on LB-agar plates and incubated over night at 37°C. Single colonies were picked the next day and used for inoculation. Plasmid DNA was isolated as described before and sent for Sanger sequencing to Seqlab/Microsynth.

2.5.10 Polymerase chain reaction (PCR)

The Platinum Pfx Polymerase (Invitrogen) was used according to the manufacturers' protocol to amplify DNA fragments via Polymerase chain reaction (PCR). Additional restriction sites were added with specifically designed primers (table 4). For genotyping purposes the GoTaq® genotype Kit (Promega) was used according to the protocol. For the Platinum Pfx Polymerase (Invitrogen) an annealing temperature of 68°C was used, the annealing temperature of the GoTaq® Polymerase was 72°C.

All PCRs were conducted according to the following protocol (X= melting temperature, primer-specific):

Table 8: PCR protocol used in this study

PCR program		
94°C	5 mins	
94°C	30 sec	25-35 cycles
X °C	45 sec	
68 or 72°C	1 min per kb	

68 or 72°C	5 min	
4°C	∞	

2.5.11 Surveyor Assay

In order to detect Cas9-mediated mutagenesis the surveyor assay was performed according to the Surveyor® Mutation Detection Kit (IDT) protocol. Primers were designed using the IDT web tool. For the nuclease assay 0.8 µg PCR product and 0.5 µl Nuclease were used in a final volume of 20 µl. The reaction was performed for 60 mins at 42°C and analyzed by loading the samples on an agarose gel.

2.5.12 Isolation of genomic DNA and RNA

Cell or organoid pellets were harvested by centrifugation, washed twice in PBS and minced using a pestle. Tissue samples were first cut into smaller pieces before using the pestle. DNA and RNA was then isolated simultaneously with the AllPrep DNA+RNA Mini Kit (Qiagen) according to the manufacturers' protocol.

2.5.13 Measuring DNA and RNA concentration

DNA or RNA concentration was measured with a NanoDrop1000 (PEQLAB) using 1 µl of DNA or RNA dissolved in ddH_2O.

2.5.14 cDNA synthesis and Quantitative Real-time-PCR (qRT-PCR)

cDNA synthesis was performed using the PrimeScript RT MasterMix (Takara) according to the manufacturers' protocol. The SYBR Premix Ex Taq (Takara) was used for qRT-PCR according to the protocol on a QPCR CFX connect (Bio-Rad). Data was analyzed with the CFX Maestro software (Bio-Rad) using the $2^{(-\Delta\Delta Ct)}$-method.

2.6 Biochemical methods

2.6.3 Whole-cell staining with propidium iodide (PI)

The Guava® easyCyte™ Plus System and Software (Luminex) was used for cell phase analysis. Before drug treatment KAP 2D cells were synchronized for 24 hours by FCS withdrawal. Following 24 hours drug treatment the cells were detached using 0.05% trypsin/EDTA working solution and adjusted to $1x10^6$ cells in 250 µl PBS. For fixation 750 µl of ice cold EtOH was added dropwise while vortexing the mixture. Cells were fixed over night at 4°C. The next day cells were washed once in 10 ml 1% BSA in PBS. The pellet was resuspended in 1 ml PBS supplemented with PI (50 µg/ml) and RNase (250 µg/ml). Before cell phase analysis cells were stained over night at 4°C.

2.6.4 Cell Titer Glo (CTG)

Organoids were split by mechanical dissociation and digested into single cells as described before. Cells were detached using 0.05% trypsin/EDTA working solution. Depending on the culture between 1000 to 2000 single cells per well were plated in all-white 96 well plates (Greiner). Organoids were plated in culture medium containing 10% Growth Factor Reduced (GFR) Matrigel™ (Corning). The treatment was started after a recovery phase of 24 hours. ATP level were measured 96 hours after drug treatment using Cell-Titer Glo2.0 reagent (Promega) according to the manufacturers' instructions. Results were normalized to vehicle (DMSO = 100%). The analysis was performed in 3 technical and biological replicates if not stated otherwise.

2.6.5 Colony formation assay

Following detachment with 0.05% trypsin/EDTA working solution 7500 KAP 2D cells per well were plated in 12 well plates. Cells were allowed to reattach for 24 hours then the treatment was started. After 96 hours of drug treatment the medium was removed and the cells were fixed in 10% PFA in MiliQ for 15 mins at RT. Fixed cells were stained with crystal violet solution (0.5% in MiliQ) for 15 mins at RT and washed

twice using MiliQ water. The colony formation assay was performed in biological duplicates.

2.6.6 TNFα ELISA

The TNFα Mouse Uncoated ELISA Kit (Thermo Fisher) was used to determine soluble TNFα level in drug treated KAP 2D cells. 100 µl of conditioned medium per well was incubated for 24 hours at 4°C on TNFα pre-coated ELISA plates. The assay was performed according to the manufacturers' protocol. The analysis was performed in 3 technical replicates.

2.6.7 Protein Isolation

Cells were washed twice in PBS and pelleted via centrifugation for 5 mins at 5000 rpm. Tissues were first minced into small pieces using scissors and a pestle. The samples were resuspended in 300 µl NP40 buffer and incubated for 10 mins on ice while inverting the tube every two to three minutes. After the incubation samples were centrifuged at 13300 rpm for 15 mins at 4°C and the protein containing supernatant was transferred into a new reaction tube and used for further analysis.

2.6.8 Measuring protein concentration

Protein concentrations were measured using the DC Protein Assay (Bio-Rad) according to the manufacturers' protocol.

2.6.9 SDS gel electrophoresis (SDS-PAGE)

SDS-PAGE was conducted to separate proteins according to their molecular weight. To prepare and run the gels the Mini-PROTEAN Tetra Vertical Electrophoresis Cell device (Bio-Rad) was used. Gels were prepared according to the web tool from cytographica.

Table 9: example for a 10% separation and a 6% stacking gel

	Separation gel (10%)	Stacking gel (6%)
solution	volume	volume
ddH^2O	3.8 ml	2.9 ml
40% Acrylamide	2 ml	750 µl
1.5 M TrisHCl pH 8.8	2 ml	x
0.5 M TrisHCl pH 6.8	x	1.2 ml
10% SDS	80 µl	50 µl
10% APS	80 µl	50 µl
TEMED	8 µl	5 µl
Final volume	8 ml	5 ml

Before loading the gels 20 to 30 µg of protein was mixed with 1/5 (v/v) 5x Laemmli buffer and filled up either to a final volume of 20 or 40 µl depending on the comb and pocket size. Proteins were then denaturated at 95°C for 8 mins. SDS Page was performed using chambers filled with 1x running buffer and the current was set to 80V for the stacking and 120V for the separation gel.

2.6.10 Western Blot

Western blot was performed using a wet blot device (Bio-Rad). First, PVDF membranes were activated in MetOH for 5 mins. Spronges, whatman paper and gels were kept wet at all times in transfer buffer. The blotting sandwich was arranged in the respective order according to the device. The transfer was performed at 100V for 90 mins at 4°C. Membranes were blocked with 5% BSA in TBST for one hour at RT and afterwards incubated with primary antibody over night at 4°C. The next day, membranes were washed three times with TBST for 5 mins each and incubated with HRP-coupled secondary antibodies for one to three hours at RT. Following the incubation with the secondary antibodies membranes were washed three times with TBST and developed using Clarity Western ECL Substrate (Bio-Rad) and the ChemiDoc Imaging System (Bio-Rad).

2.7 Animal experiments

2.7.3 Mouse husbandry

All mouse experiments that have been performed in this study have been approved by the responsible local authority (Regierungspräsidium Tübingen), Baden-Württemberg. Mice were housed in type II long cages (food and water *ad libitum)* under specific pathogen-free conditions according to the guidelines of the University of Tübingen.

2.7.4 Subcutaneous organoid injection

Organoids were digested into single cells as described before, washed twice with PBS and filtered through a 100 µm mesh. Cell counting was performed in a Neubauer chamber. The cell number was adjusted to $1x10^5$ cells in a 1:1 mixture of sterile PBS and growth factor reduced (GFR) Matrigel™ (Corning). Mice were anaesthetized using an isoflurane chamber and cells were injected into the left and right flank with a 30G needle. Mice were injected at 8 to 10 weeks of age.

2.7.5 Injection of organoids into the spleen

Organoids were digested into single cells as described before, washed twice with PBS and filtered through a 100 µm mesh. Cell counting was performed in a Neubauer chamber. The cell number was adjusted to $1x10^5$ cells in a 1:1 mixture of sterile PBS and growth factor reduced (GFR) Matrigel™ (Corning). Mice were anaesthetized using ketamine (100 mg/kg bodyweight) and xylazin (10 mg/kg bodyweight) in NaCl and a small laparotomy below the thorax was performed. The spleen was exposed and the organoid solution was injected with a 30G needle into the capsule of the spleen. Before placing the spleen back the injection site was washed once with pre-warmed PBS. The mouse was closed with resorbable suture material and individual stitches. Mice were injected at 8 to 10 weeks of age.

2.7.6 Treatment with p38α inhibitors

Eight days following subcutaneous injection mice were treated for the first time. In the splenic model the treatment start was 35 days after injection.
Mice were treated daily with 20 mg/kg vehicle, Skepinone-L or LN1639 via oral gavage. The compounds were dissolved in Cremophor/Ethanol/H_2O (12.5%/12.5%75%) and administered in 10 µl/g bodyweight.

2.8 Next generation sequencing (NGS)

For NGS DNA was isolated using the AllPrep DNA+RNA Mini Kit (Qiagen). The human CRC organoid cultures were analyzed using the Somatic Tumor Panel TUM01 library (CeGaT). The sequencing was performed using a NovaSeq 6000 device. Copy number variants (CNVs), single nucleotide variants (SNVs), insertions and deletions (INDELs) and copy number variants were analyzed by CeGaT and Dr. Thales Kronenberger.

2.9 Statistical analyses

Statistical analyses were performed using the GraphPadPrism software.

3. Results

3.1. Generation and characterization of murine CRC organoids

To analyse the role of p38α in colitis-independent, colorectal cancer, we aimed to generate murine CRC organoids. To do so, I firstly established organoids from healthy colon epithelial cells of *Kras*^{LSL} x *Trp*53$^{fl/fl}$ mice (hereinafter referred to as not transformed, NT). Within five days after isolation, the formation of three-dimensional (3D) spherical structures could be observed (Fig. 3a and b). NT organoids were analyzed via immunofluorescence (IF) and showed expression of CK20 and CDX2, two common markers of colon epithelial cells (Fig. 3c). In the next step, these colon-derived NT organoids were used to generate a CRC organoid culture. The transformation of NT organoids was achieved *in vitro* by CRISPR/Cas9-mediated gene deletion of *Apc* (transient lipofectamine transfection of pX330.Apc.2) and *cre*-mediated recombination of the floxed *Kras* and *Trp53* alleles. The transformed murine CRC *Kras*$^{G12D/+}$ x *Trp53*$^{-/-}$ x *Apc*$^{mut/+}$ culture (hereinafter referred to as Kras-Apc-p53, KAP) was selected through growth factor withdrawal. In contrast to the NT organoid culture, KAP organoids were able to grow in the absence of EGF, R-Spondin (RSPO) and Wnt (Fig. 3e). Furthermore, KAP organoids maintained a strong CK20 and CDX2 expression (Fig. 3f).

In order to generate a two-dimensional (2D) murine CRC cell culture for future experiments, KAP organoids were isolated from matrigel, fragmented via mechanical dissociation and plated without any extracellular matrix on common cell culture dishes (Fig. 3g).

To investigate whether the 2D culture conditions influence the CK20 and CDX2 expression, IF analyses were performed. Even after several passages, the 2D culture maintained the expression of the above mentioned differentiation markers CK20 and CDX2 (Fig. 3h). Finally, NT, KAP 3D and 2D cultures were further characterized on a molecular level by conducting *Kras*^{LSL} and *Trp*53$^{fl/fl}$ genotyping PCRs, as well as a surveyor nuclease assay for the detection of CRISPR/Cas9-mediated gene deletion of *Apc.* In contrast to the NT organoids, a *cre*-mediated recombination of the floxed *Kras* and *Trp53* alleles was seen in the KAP cultures.

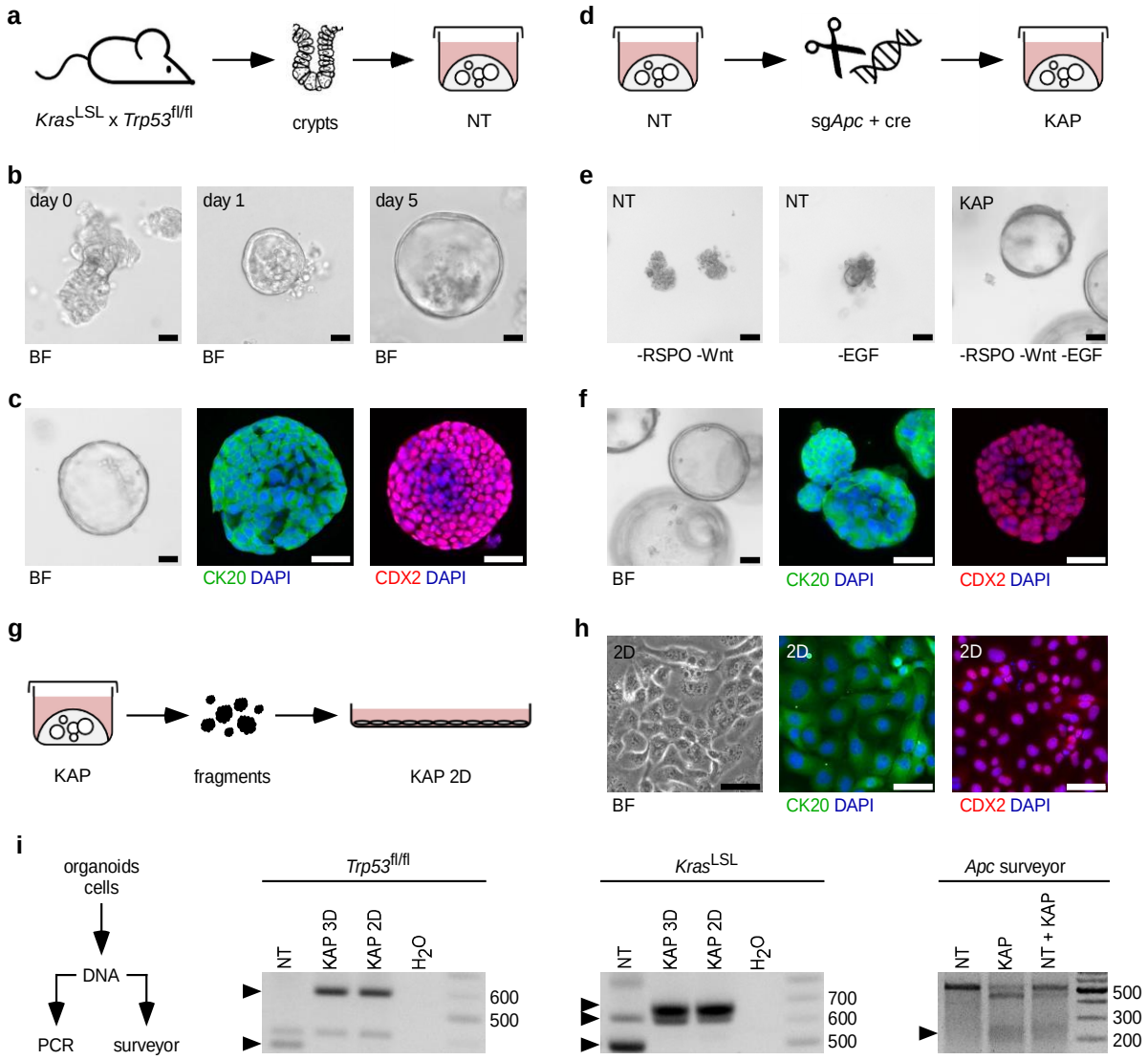

Figure 3. Generation, transformation and characterization of murine colon organoids. **(a)** Schematic illustration of the generation of *Kras*^{LSL} x *Trp*53$^{fl/fl}$ (NT) derived colon organoids. **(b)** Representative BF pictures of colonic crypts (isolation, day 0) and of NT organoids 1 and 5 days following isolation. Scale bars=50 µm. **(c)** From left representative BF picture, CK20 and CDX2 IF staining of established NT organoid culture. Scale bars=50 µm. **(d)** Schematic illustration of the Lipofectamine2000 transformation of NT organoids via CRISPR/Cas9-mediated gene deletion of *Apc* and *cre*-induced recombination of *Trp53*$^{fl/fl}$. **(e)** Selection via growth factor withdrawal of the established KAP organoid culture (right). NT organoids were used as control (left). Scale bars=50 µm. **(f)** From left representative BF picture, CK20 and CDX2 IF staining of established KAP organoid culture. Scale bars=50 µm. **(g)** Schematic illustration of the generation of a KAP organoid-derived 2D cell culture. **(h)** From left representative BF picture, CK20 and CDX2 IF staining of established KAP 2D cell line. Scale bars=50 µm. **(i)** Molecular analysis of NT, KAP and KAP 2D cultures via genotyping PCR and surveyor nuclease assay. From left schematic illustration of the workflow, *Kras*^{LSL} and *Trp*53$^{fl/fl}$ genotyping PCR and *Apc* surveyor nuclease assay. *Trp*53$^{fl/fl}$ PCR: arrow heads indicate 370 bp for the floxed and 612 bp for the recombined allele. *Kras*^{LSL} PCR: arrow heads indicate 510 bp for the floxed, 630 bp for the WT and 650 bp for the recombined allele. *Apc* surveyor: arrow head indicates 250 bp nuclease cleavage product.

The surveyor nuclease assay revealed a heterozygous cleavage in the *Apc* locus of the transformed KAP organoids, but not in the *Apc* locus of the NT organoids (Fig. 3i).

3.2. Generation and characterization of organoid-based CRC mouse models

In order to establish organoid-based CRC mouse models, KAP organoids were subcutaneously injected into the rear flanks of syngeneic immunocompetent mice (injection of $1x10^5$ organoid-derived single cells). These injections resulted in a rapid formation of macroscopically visible tumors within a week. IHC characterization of tumor samples revealed a histological phenotype that strongly resembles moderately differentiated, aggressive human CRC that are positive for Cytokeratins and CDX2 (Fig. 4a).

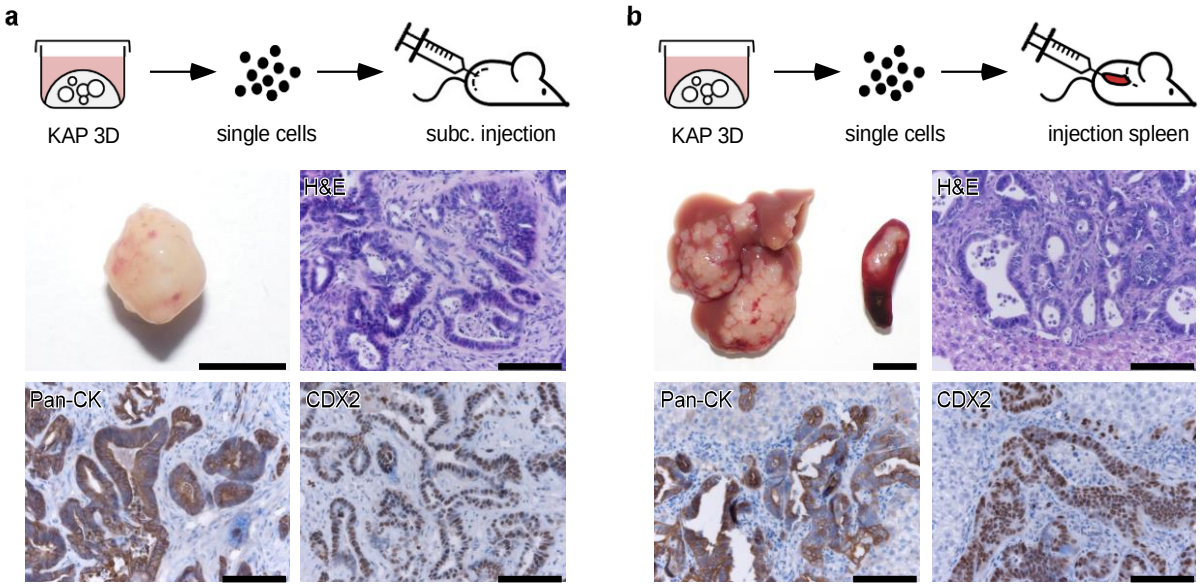

Figure 4. Generation and characterization of organoid-based CRC mouse models (a) schematic illustration of the subcutaneous injection of the KAP organoid culture into the flanks of mice (upper panel). Representative picture of KAP induced subcutaneous tumor (scale bar=0.5 cm) and IHC characterization of the tumor tissue via H&E, Pan-CK and CDX2 staining (scale bars=100 µm). **(b)** Schematic illustration of the injection of KAP organoids into the murine spleen (upper panel). Representative picture of a KAP induced primary tumor in the spleen and liver metastases (scale bar=1 cm) as well as IHC characterization of liver metastases via H&E, Pan-CK and CDX2 staining (scale bars=100 µm).

In order to test whether the KAP organoids can be also used to generate CRC metastases in the liver, we performed splenic injection of these cultures ($1x10^5$ organoid-derived single cells). In this model, the mice had to be sacrificed starting six to seven weeks after the injection due to a multinodular development of CRC metastases. A histopathological analysis of these metastases revealed moderately differentiated, aggressive tumor development in the liver (Fig. 4b).

3.3. Induction of shRNA-mediated of *Mapk14* in murine CRC cultures

To investigate the relevance and therapeutic potential of p38α inhibition in CRC, inducible shRNA-mediated knockdown of the p38α gene *Mapk14* was established in CRC organoids (together with Dr. Ramona Rudalska). Six shRNAs targeting different mRNA regions of *Mapk14* and a control shRNA (designed to bind a sequence of the sea pansy *Renilla reniformis,* shRen) were cloned into the retroviral plasmid TRE(3G)-GFP-miRE-PGK-Puro-IRES-rtTA3 (*pRT3GEPIR*) (Fig. 5a). Retroviral particles were produced via transfection of Phoenix-ECO cells and used for the stable transduction of KAP 3D and KAP 2D cells. The successfully transduced cells and organoids were selected with puromycin and shRNA cassette expression was induced with doxycycline. To determine the knockdown efficacy of these shRNAs, p38α protein level were analyzed four days following shRNA induction (in comparison to shRen) in KAP 2 D cells. While induction of two shRNAs (1416 and 2131) resulted only in a moderate knockdown of *Mapk14*, a strong reduction of p38α protein level was seen with three shRNAs (2486, 2605 and 2948 (Fig. 5b)).

To measure whether reduction of p38α protein level leads to a reduced viability of colitis independent CRC, we treated KAP 3D cells for 10 days with doxycycline and subsequently performed cell viability analyses. While a weak knockdown of *Mapk14* only moderately influence CRC organoids, we found strongly reduced viability of KAP 3D cells upon pronounced knockdown of *Mapk14* (compared to shRen cells, 100 % viability, Fig. 5c).

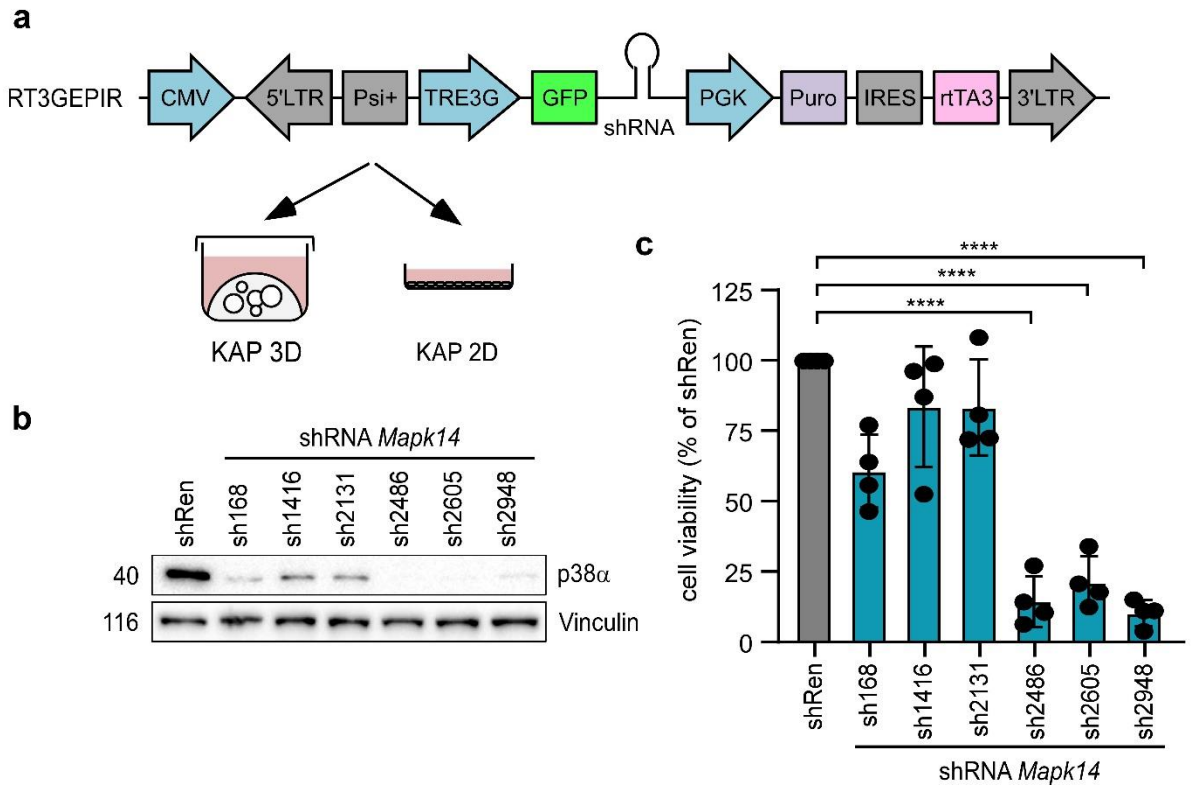

Figure 5. Analysis of shRNA-mediated *Mapk14* knockdown in KAP 2D and 3D cultures **(a)** Schematic illustration of the retroviral RT3GEPIR plasmid used for the stable transduction of KAP 2D and KAP 3D cells. The vector consists of the cytomegalovirus *(*CMV*)* immediate early enhancer and promoter, 5' and 3' long terminal repeats (LTR), a packaging signal (Psi+), a Tet-on promotor of the 3rd generation (TRE3G), the green fluorescent protein (GFP), the mirE-cassette embedded control or *Mapk14* shRNA, a phosphoglycerate kinase promotor (PGK) driven puromycin (Puro) resistance cassette, an internal ribosome entry site (IRES) and the reverse tetracycline-controlled transactivator 3 (rtTA3).**(b)** Western Blot analysis of transduced and selected KAP 2D cells four days after shRNA induction with doxycycline. Vinculin was used as loading control. **(c)** Cell viability analysis using CTG twelve days after shRNA induction with doxycycline (KAP 3D). Cell viability was normalized to shRen control cells. p-value <0.0001 (unpaired t-test). Data is depicted as mean with SD, n=4 (biological replicates).

Taken together, these data show that pronounced knockdown of *Mapk14* results in a strongly reduced viability of colitis independent CRC cultures.

3.4. Therapeutic potential of selective p38α kinase inhibitors in organoid based *in vitro* and *in vivo* CRC models

Based on the observed therapeutic effect of shRNA-mediated knockdown of *Mapk14* in murine CRC organoids, I next tested the outcome of pharmacological p38α inhibition in these cultures. Increasing concentrations of the two selective and established p38α inhibitors Skepinone-L (SKL) and PH797804 (PH) [85, 86] were used to conduct viability assays (CTG) in KAP 3D and 2D cultures. Even at high concentrations, both inhibitors only showed a moderate induction of cell death in both cultures (Fig. 6a). This finding was confirmed with a colony formation assay performed in KAP 2D cells (using a 5 µM concentration of compounds, Fig. 6b).

In order to analyze whether these inhibitors allow for efficient inhibition of p38α signaling, the activity of p38α and two well-established p38α downstream targets (HSP27, MAPKAPK-2 [26]) were analyzed. KAP 2D cells were treated for 24, 48 and 72 hours and subjected to western blot analysis. Interestingly, these analysis revealed higher activity of p38α (P-p38$^{Thr180/Tyr182}$) and upregulation of total and phosphorylated MAPKAPK-2 (MK2) level upon treatment. No relevant effects on active HSP27 (P-HSP27^{Ser82}) could be observed after 72 hours' of treatment (Fig. 6c).

It was shown that p38α influences the microenvironment of tumors *in vivo* [87, 88]. To test the therapeutic effect, of specific p38α inhibition *in vivo*, I applied the previous established, organoid-based CRC mouse models. KAP organoids were subcutaneously injected into immunocompetent mice and treated daily with vehicle or SKL starting eight days after organoid injection. The analysis of tumor growth during treatment showed no significant effect of Skepinone-L in this model (Fig. 6d). In order to analyze the treatment response in CRC metastasis, KAP organoids were injected into the spleen of WT mice. The vehicle or SKL treatment was started five weeks (day 35) after splenic injection and a survival analysis was conducted. The SKL treatment did not lead to a significant survival benefit (Fig. 6e).

To analyze the effect of Skepinone-L on p38α signaling *in vivo*, western blot analysis on protein lysates isolated from liver metastasis following a four day treatment with vehicle or SKL was performed. In line with the *in vitro* findings, an upregulation of

active p38 (P-p38$^{Thr180/Tyr182}$), could be observed, while no influence on MK2 activity was detected (Fig. 6f).

In summary, these data indicate that pharmacological inhibition of p38α, using established and selective p38α inhibitors such as Skepinone-L or PH results in upregulation of p38α and did not phenocopy the results of genetically induced p38α loss in colitis-independent CRC.

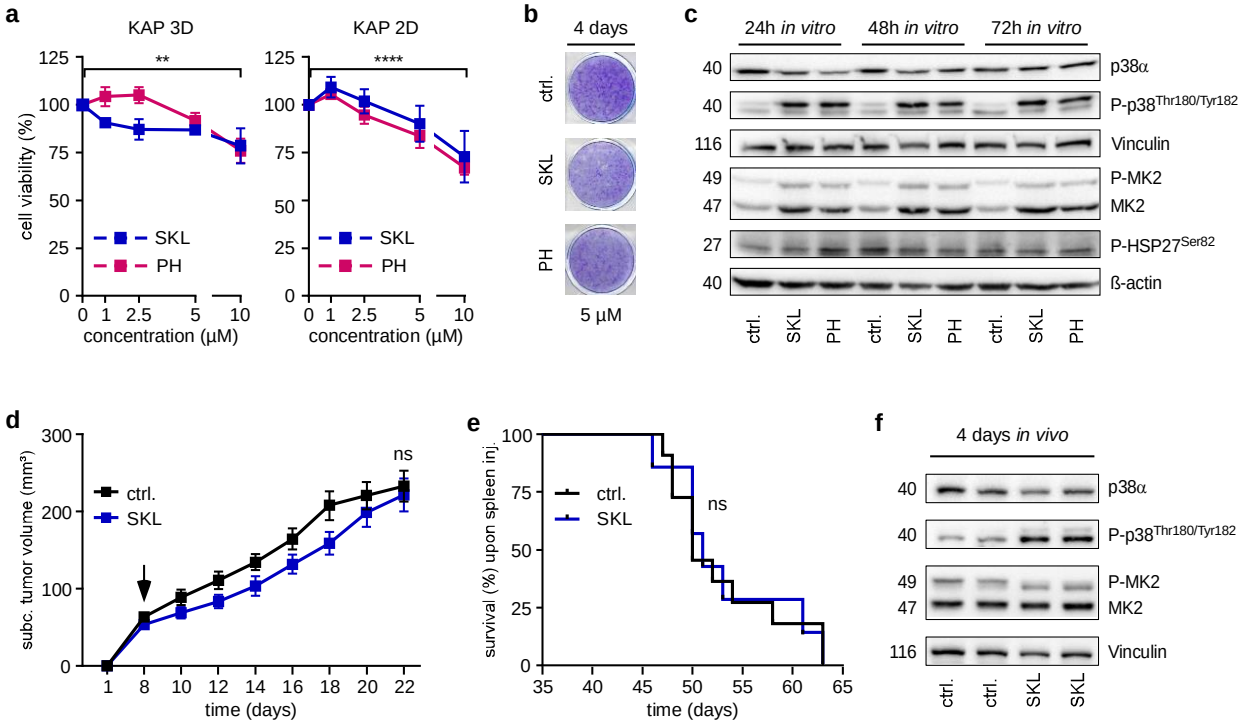

Figure 6. Analysis of the selective p38α inhibitors Skepinone-L and PH797804 in CRC organoid models (*in vitro* and in *vivo*) (a) Cell viability analysis using CTG of KAP 3D and 2D cultures treated with SKL or PH for four days. Cell viability was normalized to DMSO treated control. Statistical analysis: two-way ANOVA, Dunnett's multiple comparisons test. KAP 3D: SKL p-value=0.0151, PH p-value=0.0063. KAP 2D: SKL and PH p-value<0.0001. Data is depicted as mean with SD. n=3 (biological replicates) **(b)** Colony formation assay for SKL or PH treated KAP 2D cells. Cells were treated for 4 days at a 5 µM concentration. **(c)** Western blot analysis of p38α and its downstream targets upon treatment with DMSO, SKL or PH. Time course after 24, 48 and 72 hours of treatment at a concentration of 5 µM (KAP 2D). Vinculin and β-actin were used as loading controls. **(d)** SKL treatment response in the subcutaneous tumor model. KAP organoids were injected into the flanks of *Trp*53$^{fl/fl}$ mice. Eight days after injection mice were treated daily with vehicle or SKL (arrow). Statistical analysis: two-way ANOVA, Dunnett's multiple comparisons test. p-value=0.7346 (ns). Vehicle n=7, SKL n=9. Data is depicted as mean with SEM. **(e)** Survival analysis in the liver metastasis model. KAP organoids were injected into the spleen of WT mice. Five weeks after injection mice were treated daily with vehicle or SKL. Statistical analysis: Log-rank (Mantel-Cox) test. p-value=0.9482 (ns). Vehicle n=11, SKL n=7. **(f)** Western blot analysis of protein lysates isolated from liver metastases of vehicle or SKL treated mice (four days treatment). Vinculin was used as a loading control. n=2 (biological replicates).

3.5. Therapeutic analysis of the next generation p38α inhibitor LN1639

SKL was published in 2011 [85] and has been used as a lead compound for the development of next generation p38α inhibitors with optimized target residence times. One of these newly synthesized compounds is the type 1.5 p38α kinase inhibitor LN1639 (1639) (target residence time 259 s in comparison to 150 s for SKL). In order to test whether 1639 allows for an increased therapeutic effect in CRC, this compound was tested side by side with SKL in a CTG cell viability assay. In contrast to SKL, 1639 treatment lead to a dose dependent induction of cell death in KAP 3D and 2D cultures (Fig. 7a). To also test the effect of 1639 on cell proliferation, an EdU incorporation assay was conducted. I found that 1639 treated cells showed a significant reduction of cells undergoing S-phase (25% reduction compared with DMSO treated control) (Fig. 7b). In line with these data, 1639 strongly reduced the formation of colonies of KAP 2D cells (2.5 µM concentration, Fig. 7c).

To test the therapeutic effect of 1639 *in vivo*, I took advantage of the previously described CRC mouse models. Immunocompetent mice were subcutaneously injected with KAP organoids and treated daily with vehicle, SKL or 1639. After 8 days of 1639 treatment (day 16) a significant reduction of subcutaneous tumor volume could be observed when compared to vehicle treated mice (Fig. 7d). Furthermore, 1639 treatment also resulted in a moderate survival benefit in the KAP organoid based metastasis model. In comparison to vehicle treated mice, the median survival was increased from 50 to 61 days (p-value = 0.1623, Fig. 7e). All mice tolerated the treatment well as no effects on general health or drastic influences on weight development could be observed (Fig. 7f).

Taken together, these data indicate that only p38α inhibitors with increased target residence time show a therapeutic benefit against colitis-independent CRC.

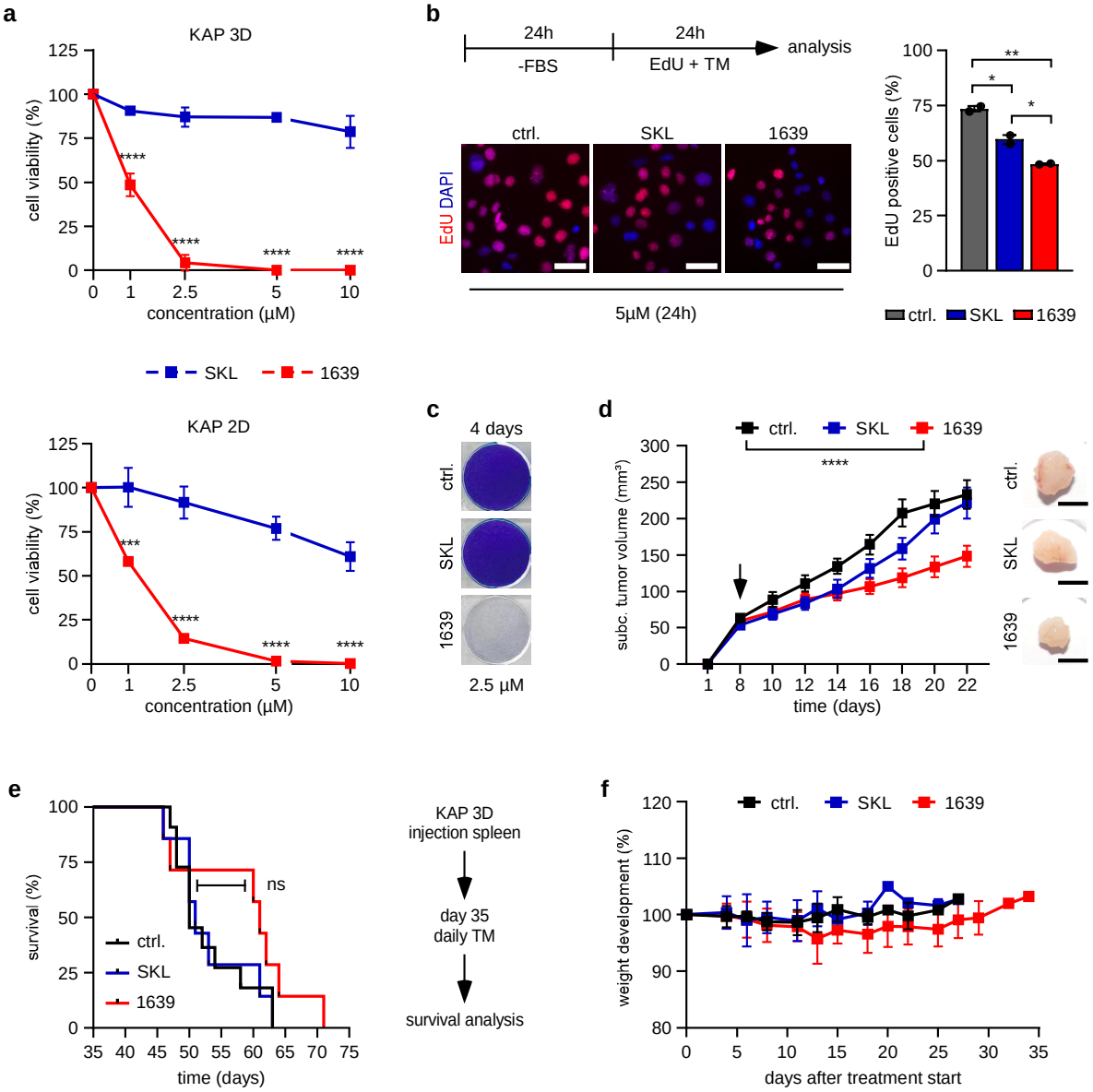

Figure 7. Analysis of the next generation p38α inhibitor LN1639 in comparison with SKL. (a) Cell viability analysis using CTG of KAP 3D and 2D cultures treated with SKL or 1639 for four days. Cell viability was normalized to DMSO treated control. Statistical analysis: two-way ANOVA, Sidak's multiple comparisons test (SKL vs.1639). *** p-value=0.002, **** p-value <0.0001. Data is depicted as mean with SD. n=3 (biological replicates) **(b)** EdU proliferation assay for cell phase analysis. Schematic illustration of the workflow (upper panel). Representative pictures of DMSO, SKL or 1639 treated KAP 2D cells (lower panel). EdU positive cells were normalized to total cells (DAPI). Two biological replicates (right panel). Statistical analysis: unpaired t-test. Ctrl. vs. SKL p-value=0.0267, Ctrl. vs. 1639 p-value=0.0025, SKL vs. 1639 p-value=0.0318. **(c)** Colony formation assay for SKL or 1639 treated KAP 2D cells. Cells were treated for 4 days with 2.5 µM. **(d)** SKL and 1639 treatment response in the subcutaneous tumor model. KAP organoids were injected into the flanks of *Trp*53$^{fl/fl}$ mice. Eight days after injection mice were treated daily with vehicle, SKL or 1639 (arrow). Representative pictures of subcutaneous tumors on day 22 (scale bar=0.5 cm) Statistical analysis: two-way ANOVA, Dunnett's multiple comparisons test. p-value <0.0001. Vehicle n=7, SKL n=9, 1639 n=10. Data is depicted as mean with SEM. **(e)** Survival analysis in the liver metastasis model. Five weeks after injection, mice were treated daily with vehicle, SKL or 1639. Statistical analysis: Log-rank (Mantel-Cox) test. p-value=0.1623. Vehicle n=11, SKL n=7, 1639 n=7. **(f)** Weight development upon treatment in the liver metastasis model. The weight was normalized to the first day of the treatment (day 0, 100%). n=7 each.

3.6. Analysis of p38α downstream targets and TNFα level upon SKL or 1639 treatment

To examine the different therapeutic effects of 1639 and SKL in CRC, I next performed western blot analysis of p-p38α and p38α downstream targets under treatment. Interestingly, I found that 1 µM of 1639 lead to an even stronger activation of p38α and MK2 than SKL, although a severe induction of apoptosis (cleaved caspase 3) was detected. Phosphorylation of ATF2 and HSP27 was increased within 24 and 48 hours of 1639 treatment, however, reduced at the 72 hours' time point (Fig. 8a).

The p38α MAPK pathway is known to be activated by several secreted factors, such as TNFα [28, 89]. To test, whether p38α inhibition leads to secretion of factors, which in turn activate p38α, an experiment with conditioned medium was conducted. KAP 2D cells were treated for four hours with 1 µM DMSO, SKL or 1639. Subsequently, the cells received fresh medium without any compound. After additional four hours the conditioned medium was harvested, transferred to fresh KAP 2D cells and incubated for eight hours. Both, the SKL and 1639 treated cells as well as the corresponding conditioned medium treated cells showed a strong upregulation of p38 phosphorylation (Fig. 8b). These results suggest that a paracrine signaling mechanism might be involved in the upregulation of p38α upon treatment with p38α inhibitors.

To see, whether SKL and 1639 induce secretion of TNFα in CRC, KAP 2D cells were treated for 8 and 24 hours, either with 1 or 5 µM DMSO, SKL or 1639 and TNF secretion was analyzed by an ELISA assay. While the basic level of TNFα in the medium of KAP 2D cells was low, I found a significantly upregulated TNFα secretion upon treatment with 1639 (Fig. 8c). To analyze whether p38α inhibition results in a transcriptional activation of TNFα, I performed qRT-PCR analyses upon treatment of KAP 2D cells with DMSO, SKL or 1639 or upon shRNA-mediated knockdown of *Mapk14*. In both experiments, loss of p38α activity triggered a significant upregulation of *Tnfα* mRNA level (Fig. 8d, e).

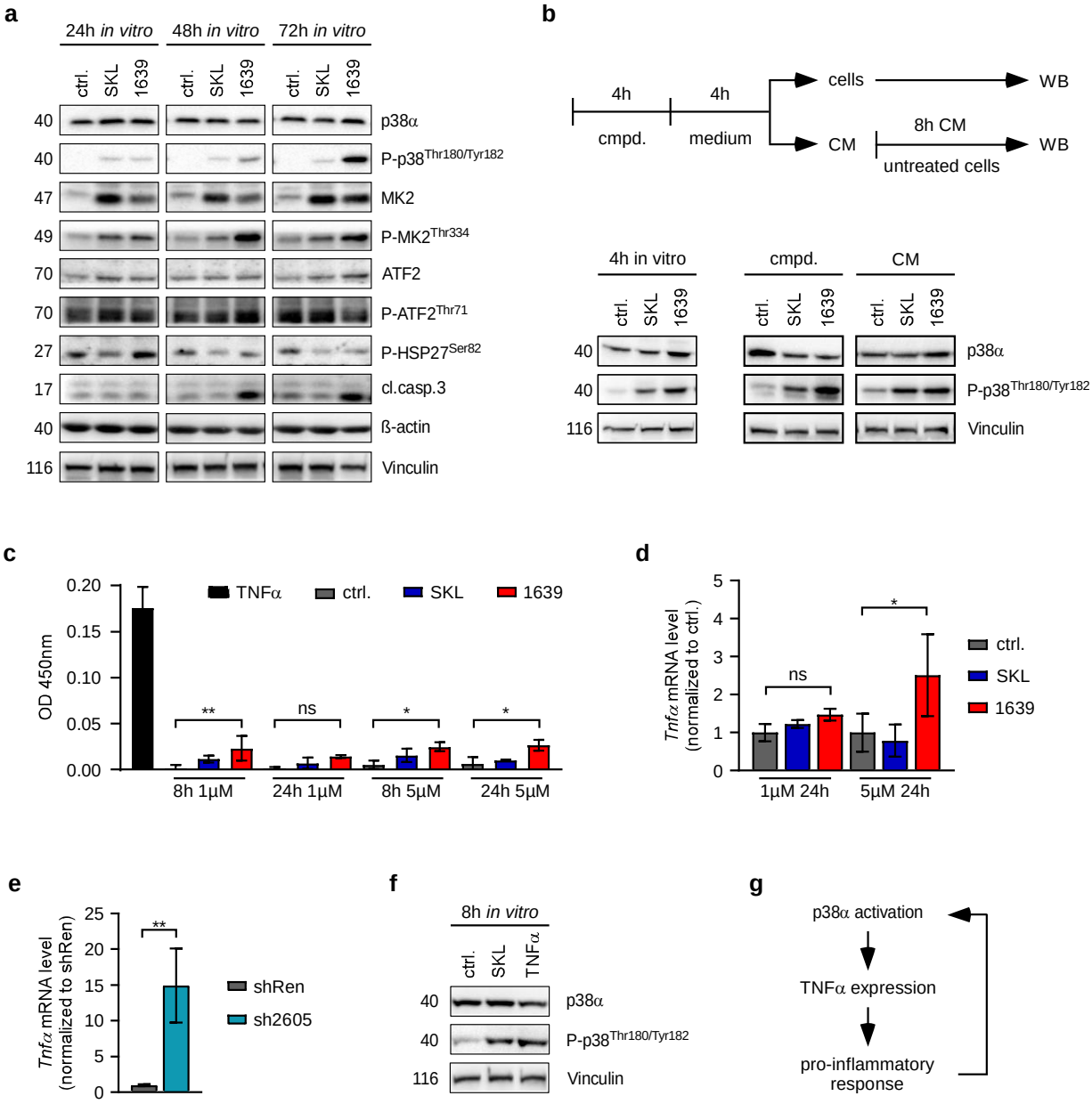

Figure 8. Influence of SKL and 1639 on p38α downstream targets and Tnfα level *in vitro*. **(a)** Western blot analysis of p38α and its downstream targets upon treatment with DMSO, SKL or 1639. Time course after 24, 48 and 72 hours of treatment at a concentration of 1 µM (KAP 2D). Vinculin and β-actin were used as loading controls. **(b)** Schematic illustration of the conditioned medium experiment workflow (upper panel). Western Blot analysis of KAP 2D cells treated for four hours with DMSO, SKL or 1639 at a 1 µM concentration (left panel). Western blot analysis of compound (cmpd.) treated KAP 2D cells (1 µM), used for the production of conditioned medium (CM) and CM treated KAP 2D cells. Total p38α and phosphorylated p38 protein level were measured, Vinculin was used as a loading control. **(c)** Conditioned media of KAP 2D cells treated with DMSO, SKL or 1639 analyzed with a TNFα ELISA. 8 pg TNFα were used as control. Absorbance was measured at 450 nm OD. Statistical analysis: one-way ANOVA, Sidak's multiple comparisons test. p-values from left: 0.0066 (*), 0.2494 (ns), 0.0169 (*), 0.0146 (*). Data is depicted as mean with SD n=3 (technical replicates). **(d)** qRT-PCR analysis of *Tnfα* expression upon DMSO, SKL or 1639 treatment (KAP 2D). mRNA levels were normalized to β-actin, *Tnfα* mRNA expression was normalized to DMSO treated control cells. Statistical analysis: two-way ANOVA, Sidak's multiple comparisons test. p-values from left: 0.8342 (ns), 0.0225 (*). Data is depicted as mean with SD, n=3 (technical replicates). **(e)** qRT-PCR analysis of *Tnfα* expression six days

after shRNA induction with doxycycline. mRNA levels were normalized to β-actin, *Mapk14* mRNA expression was normalized to shRen control cells. p-value=0.0096 (unpaired t-test). Data is depicted as mean with SD, n=3 (technical replicates). **(f)** Western blot analysis of p38α upon treatment with DMSO, SKL (5 µM) or recombinant TNFα (20 ng/ml) for 8 hours (KAP 2D). **(g)** Schematic illustration of the p38α/TNFα feedback loop (left panel).

To investigate whether TNFα induces phosphorylation of p38α in KAP 2D cells, the cells were treated with recombinant TNFα for 8 hours and western blot analysis was performed. Indeed, an upregulation of active p38 comparable to a 5 µM SKL treatment could be observed (Fig. 8f).

Taken together, I found that p38α inhibition triggered increased expression and secretion of TNFα in CRC cells, which induces a paradoxical activation of p38α signaling upon treatment (Fig. 8g). Furthermore, my data indicate that the therapeutic effect of p38α inhibitors might be independent of the important p38α downstream targets MK2 and ATF2.

3.7. Analysis of pro-inflammatory cytokines connected to the p38α signaling pathway

TNFα is known to induce death of tumor cells [90, 91]. To see whether the increased expression and secretion of TNFα is responsible for the therapeutic effect of p38α blockade, a CTG viability assay with recombinant TNFα in the presence or absence of p38α knockdown was performed. KAP 2D, KAP 2D-shRen and KAP 2D-shMapk14.2605 cells were treated for four days with doxycycline and then incubated with recombinant TNFα for additional four days. Although recombinant TNFα was able to significantly decrease the viability of KAP 2D cells, the effect was mediocre and not comparable with the potency of 1639 treatment (Fig. 9a). These results suggest that the activation of TNFα itself is not responsible for the therapeutic effect of 1639.

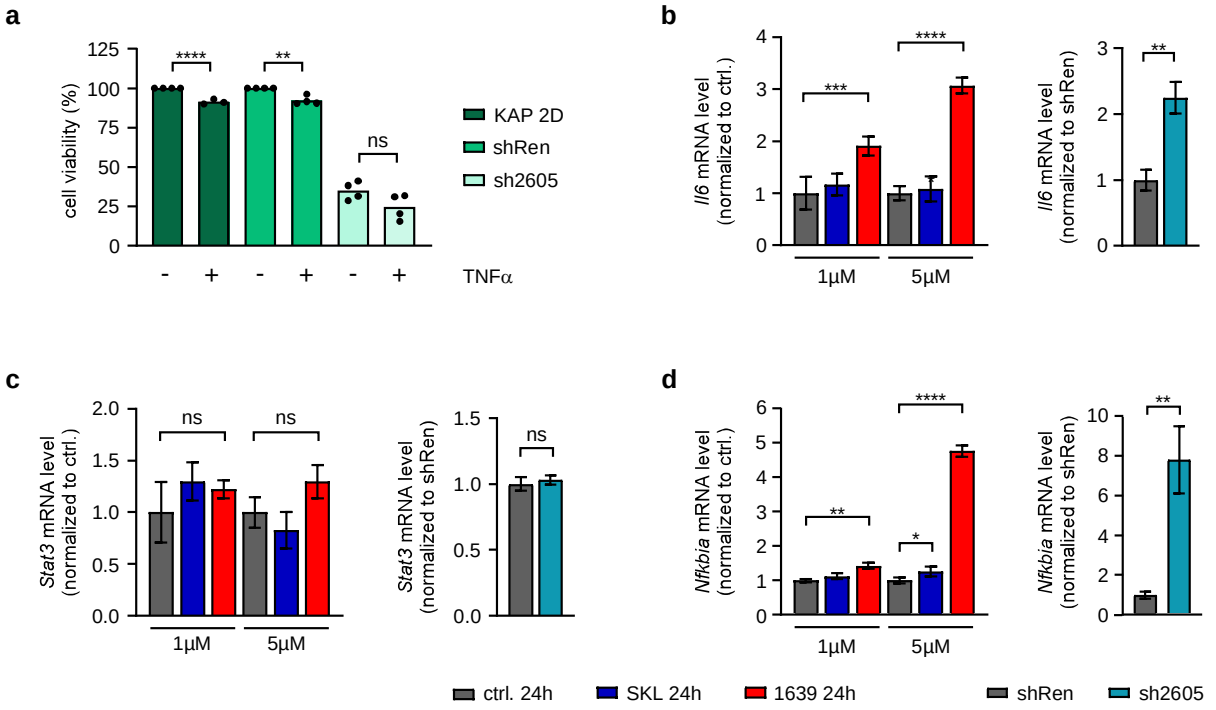

Figure 9. Influence of SKL and 1639 treatment on pro-inflammatory cytokines *in vitro.* **(a)** Cell viability analysis using CTG of KAP 2D, shRen or sh2605 cells treated with vehicle or recombinant TNFα (20 ng/ml) for 4 days. Cell viability was normalized to vehicle treated control. Statistical analysis: unpaired t-test. p-values from left: <0.0001 (****), 0.0011 (**), 0.0853 (ns). Data is depicted as mean with SD. n=4 (biological replicates). **(b-d)** qRT-PCR analysis of *Il6, Stat3* and *Nfkbia* expression upon DMSO, SKL or 1639 treatment (KAP 2D). mRNA levels were normalized to β-actin, mRNA of interest expression was normalized to DMSO treated control cells. Statistical analysis: two-way ANOVA, Sidak's multiple comparisons test. *Il6* p-values from left: 0.0009 (***), <0.0001 (****). *Stat3* p-values from left: 0.5097 (ns), 0.2605 (ns). *Nfkbia* p-values from left: 0.0019 (**), 0.0471 (*), <0.0001 (****). qRT-PCR analysis of *Il6, Stat3* and *Nfkbia* expression six days after shRNA induction with doxycycline. mRNA level were normalized to β-actin, mRNA expression of interest was normalized to shRen control cells. Statistical analysis: unpaired t-test. *Il6* p-value=0.0017 (**), *Stat3* p-value=0.4484 (ns), *Nfkbia* p-value=0.0022 (**). Data is depicted as mean with SD, n=3 (technical replicates).

I also analyzed the transcriptional activation of *Il6* and *Stat3* upon treatment with different concentrations of 1639 and SKL or shRNA-mediated knockdown of Mapk14 via qRT-PCR. Additionally, mRNA levels of the *Nf-κb* signaling pathway inhibitory subunit *Nfkbia* were investigated, since the pathway can also be activated through TNF receptor (TNFR) stimulation [92]. An increase in *Nfkbia* hereby directly correlates with an upregulation of *Nf-κb* [93, 94]. Significantly higher *Il6* and *Nfkbia* mRNA levels were detected in 1639 treated KAP 2D cells as well as in doxycycline

induced sh2605 cells (Fig. 9b, d). In contrast to *Gupta et al. 2014*, no effects on *Stat3* mRNA level were observed (Fig. 9c).

3.8. Influence of 1639 on cell cycle and DNA damage *in vitro*

TNFα and *Nf-κb* are involved in the regulation of a variety of signaling pathways and present key mediators of the cellular stress response. Their cellular regulation is intertwined with the p38α MAPK pathway and at least TNFα is able to regulate p38α activity in a positive feedback loop (Fig. 8f, g). Besides its important role in stress-mediated cellular responses, p38α also acts as mediator of controlled entry into mitosis. Immunofluorescence analyses revealed that phosphorylated and thereby activated p38α localizes at centrosomes during spindle assembly [95]. To investigate the effect of TNFα/p38α acceleration on cell cycle progression, IF analysis of p38α and its direct downstream target MK2 was conducted. Both kinases were localized at the mitotic spindle (Fig. 10a).

In eukaryotic cells, the mitotic onset is controlled by cyclin-dependent kinase 1 (CDK1) activity [96]. Since p38α was described to reduce the activity of the CDK1 upstream regulator Cdc25, causing a cell cycle delay or a cell cycle arrest upon cellular stress [97], I next analyzed the activity of CDK1 upon p38α inhibitor treatment. KAP 2D cells were treated with DMSO, SKL or 1639 for 8 and 24 hours at concentrations of 1 and 5 µM and CDK1 activity was determined by western blot analysis of the inhibitory Tyr15 phosphorylation. Treatment of CRC cells with 1639, lead to a decreased $CDK1^{Tyr15}$ phosphorylation, hence an increased CDK1 activation. The effect was more pronounced after 24 than 8 hours. In contrast, SKL treatment did not result in any detectable changes of CDK1 activity (Fig. 10b).

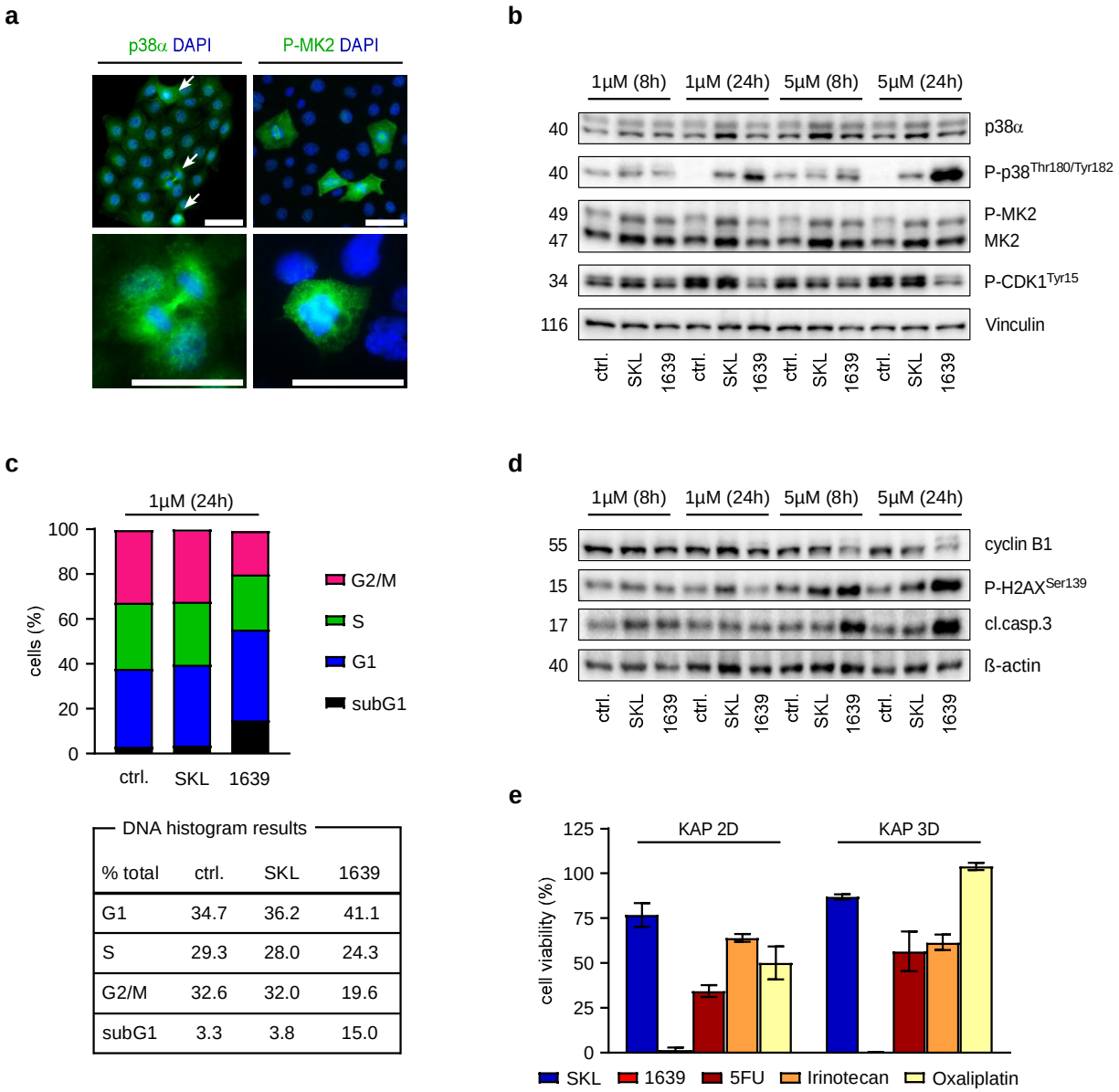

Figure 10. Cell cycle and DNA damage analysis in SKL and 1639 treated KAP 2D cells. **(a)** p38α and P-MK2 IF staining of KAP 2D cells. Arrows indicate dividing cells. Scale bars=50 µm. **(b)** Western blot analysis upon treatment with DMSO, SKL or 1639. KAP 2D cells were treated for 8 and 24 hours at a concentration of 1 and 5 µM. Vinculin was used as a loading control. **(c)** Cell cycle analysis using whole-cell staining, PI. Following synchronization via FCS withdrawal for 24 hours, KAP 2D cells were treated with 1 µM DMSO, SKL or 1639 for additional 24 hours. Statistical analysis: two-way ANOVA, Dunnett's multiple comparisons test. **(d)** Western blot analysis upon treatment with DMSO, SKL or 1639. KAP 2D cells were treated for 8 and 24 hours at a concentration of 1 and 5 µM. β-actin was used as a loading control. **(e)** Cell viability analysis using CTG of KAP 3D and 2D cultures treated with SKL, 1639, 5'FU, Irinotecan or Oxaliplatin for four days (5 µM concentration). Cell viability was normalized to DMSO treated control. n=3 (biological replicates).

Due to the fact that the treatment with 1639 enhanced CKD1 activity, a cell cycle analysis was performed. KAP 2D cells were synchronized by FCS starvation for 24 hours and subsequently treated with DMSO, SKL and 1639. Interestingly, this cell cycle analysis showed an increase in the subG1 (from 3.3 to 15%) and a decrease in the G2/M (from 32.6 to 19.6%) phase of the cell cycle (Fig. 10c). To validate these results, the protein levels of Cyclin B1 (a marker for late G2 and M phase of the cell cycle) were analyzed. Reduced level of cyclin B1 upon 24h of 1639 treatment (5 µM concentration) indicates that 1639 accelerates the G2/M transition of CRC cells (Fig. 10c). Furthermore, I found increased level of DNA damage induction (p-yH2ax) and increased level of apoptosis (cleaved caspase 3, and subG1 cells Fig. 10c, b) upon treatment with 1639.

Taken together, these data indicate, that the treatment of CRC cells with a p38α inhibitor with a long target residence time (such as 1639) impacts the cell cycle control at the G2/M transition under cellular stress, resulting in DNA damage and subsequently apoptosis of CRC cells.

Of note, DNA damage inducing chemotherapies are already established for the treatment of colorectal cancer patients [17, 18]. In order to compare the therapeutic efficacy of efficient p38α inhibition and established chemotherapies in CRC, a CTG viability assay was conducted to analyze the treatment response of SKL, 1639, 5'FU, Irinotecan and Oxaliplatin in KAP 2D and 3D cultures. Cells were treated for four days at a 5 µM concentration. Under these conditions 1639 nearly eradicated 100% of the cells, while only weak therapeutic effects were seen with the chemotherapeutic agents and SKL (Fig. 10d).

3.9. Generation and treatment response analysis of additional CRC murine organoids

Colorectal tumors can arise from various driver mutations, making CRC to a heterogeneous disease [7, 98]. In order to validate the striking therapeutic potential of 1639 in CRC organoids with different genetic makeups, two additional murine colon cancer organoid cultures were established (in collaboration with Agata Dylawerska). *Kras*$^{G12D/+}$ x *Trp53*$^{-/-}$ x *Myc*^{OE} organoids (hereinafter referred to as Kras-Myc-p53, KMP) were generated by a *cre*-mediated recombination of *Kras*^{LSL} x *Trp53*$^{fl/fl}$ (NT) organoids (Lipofectamine-mediated transfection of *cre*). The resulting *Kras*$^{G12D/+}$ x *Trp53*$^{-/-}$ culture was further transformed by using a transposable element. The cells were transfected with a transposon plasmid encoding for *Myc* under the expression of the CAG promotor (pT-Ca-*Myc*) and the sleeping beauty 13 (SB13) transposase (to induce a stable integration of CAG-Myc. (Fig. 11a). KMP organoids were selected via withdrawal of WNT and verified using genotyping PCRs for *Kras*, *Myc* and *Trp53* (by A.D.).

To generate CRC organoids, with constitutive active *Braf* mutation (*Braf*^{V600E}), firstly loss of *Apc* was induced through *cre*-mediated recombination (Lipofectamine-mediated transfection of *cre*) in the *Apc*$^{fl/fl}$ organoid culture. Next, loss of *Trp53* was induced by CRISPR/Cas9-mediated gene deletion of *Trp53* (by Lipofectamine transfection of pX330.sg*Trp53*). These organoids were infected with retroviral particles encoding for *Braf*^{V600E} using the Phoenix-ECO system (Fig. 11b). The resulting *Apc*$^{-/-}$ x *Trp53*$^{mut/mut}$ x *Braf*^{V600E} culture (hereinafter referred to as Braf-Apc-p53, BAP) was selected with puromycin and analyzed via genotyping PCR (*Apc*, *Braf*) and the surveyor nuclease assay (*Trp53*) on a molecular level (by A.D.).

Both, KMP and BAP organoids, were tested regarding their treatment response towards SKL and 1639 in the CTG viability assay. Similar to KAP organoids, 1639 treatment lead to a significant reduction of cell viability of KMP and BAP organoids, whereas SKL remained ineffective at a 5 µM concentration (Fig. 11c, d). Comparing the treatment response of all tree murine CRC organoid cultures, BAP organoids show a slightly lower sensitivity to 1639 than the other cultures. Nevertheless, this data highlights that the potency of 1639 in CRC of different genotypes.

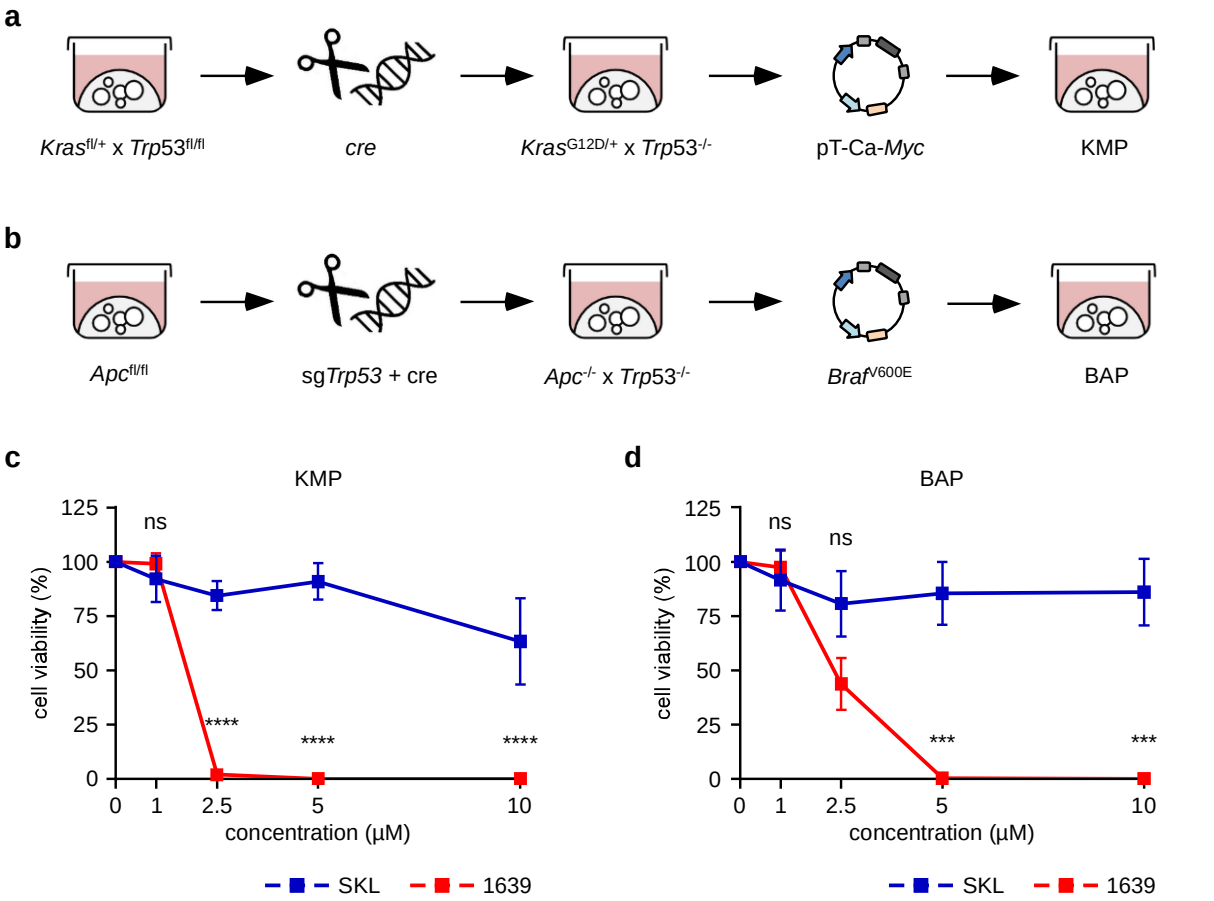

Figure 11. Generation of additional murine CRC organoids and treatment response towards SKL and 1639. (a) Schematic illustration of the Lipofectamine transfection with *cre* and retroviral transduction with pT-Ca-*Myc* to establish KMP organoids. **(b)** Schematic illustration of the Lipofectamine transfection with *cre* and sg*Trp53* followed by retroviral transduction with *Braf*^{V600E} to establish BAP organoids. **(c-d)** Cell viability analysis using CTG of KMP or BAP cultures treated with SKL or 1639 for four days. Cell viability was normalized to DMSO treated control. Statistical analysis: two-way ANOVA, Sidak's multiple comparisons test (SKL vs.1639). KMP p-values from left: 0.9820 (ns), <0.0001 (****). Data is depicted as mean with SD. n=3 (biological replicates). BAP p-values from left: 0.9977 (ns), 0.1421 (ns), 0.0008 (**), 0.0008 (**). Data is depicted as mean with SD. n=2 (biological replicates).

3.10. Patient derived CRC organoids: generation, characterization and molecular analysis

In order to test the potential of p38α inhibition in human CRC (hCRC) a panel of patient-derived CRC organoid cultures was established and characterized. In close collaboration with the surgery, the pathology and internal medicine departments of the University Hospital Tuebingen (Dr. Can Yurttas, Prof. Dr. Alfred Königsrainer, Prof. Dr. Michael Bitzer etc), two tumoroid cultures (hCRC3 and hCRC7) were generated from primary colon tumor tissue. IHC characterization via H&E, Pan-CK and CDX2 staining revealed both tumors to be moderately to well differentiated (Fig. 12a). An additional culture was established from ascites material derived from a patient, suffering from metastatic CRC (hCRC5). All three tumoroid cultures were growing consistently and showed high CK20 and CDX2 expression, even after several passages (Fig. 12b).

For a molecular analysis of these tumoroids, DNA was isolated and an exome sequencing using the somatic tumor panel TUM01 (CeGaT) was performed. Copy number variants (CNVs), single nucleotide variants (SNVs), insertions and deletions (INDELs) and copy number variants for roughly 700 genes were analyzed (in collaboration with CeGaT and Dr. Thales Kronenberger). The analysis revealed that all three cultures had loss of function mutations in the *APC* and *TRP53* loci. Furthermore a *MYC* amplification was found in hCRC5 culture and a missense mutation in the *BRAF* gene was detected in the hCRC7 culture (Fig. 12c).

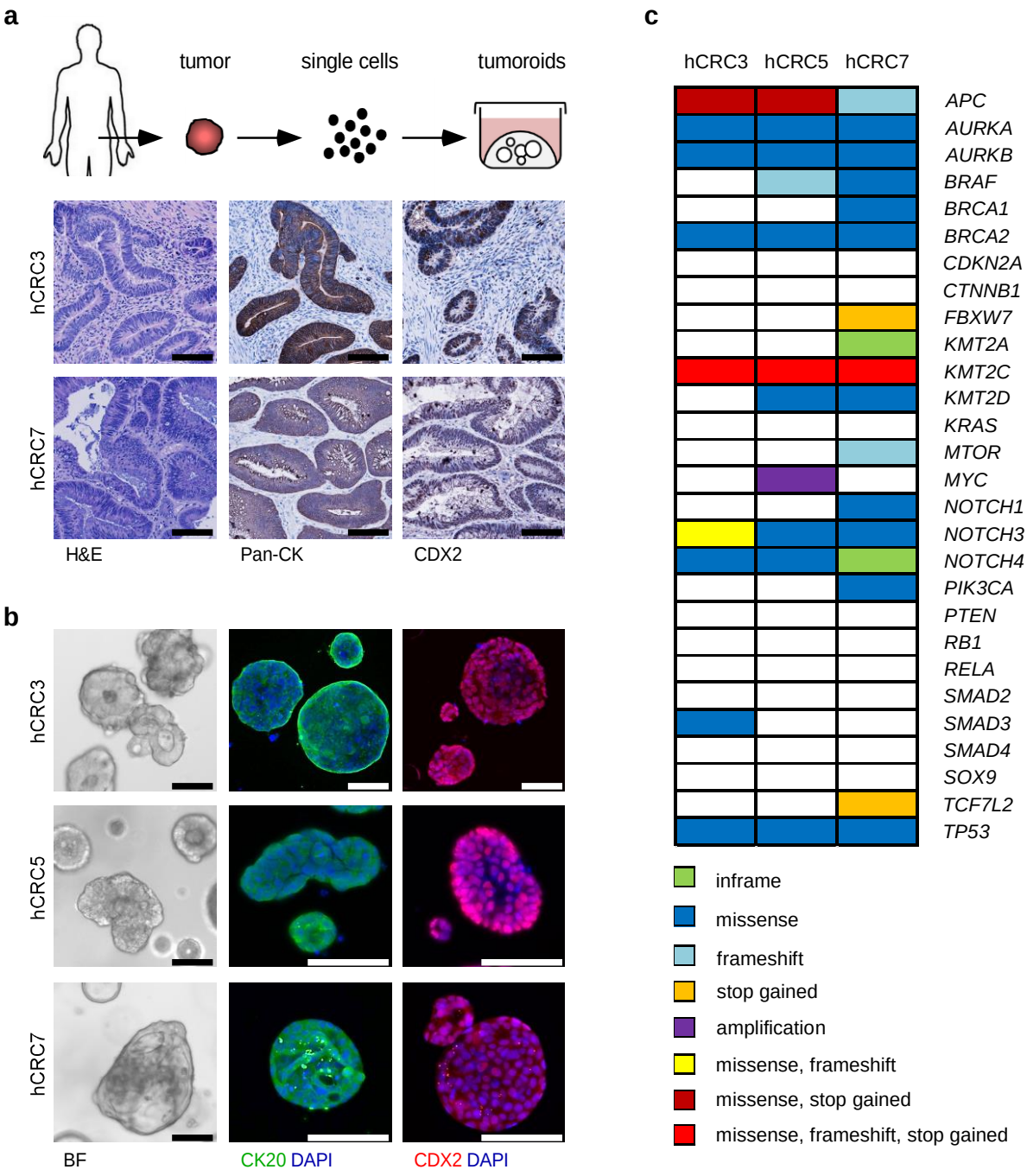

Figure 12. Patient derived CRC organoids: generation and characterization (a) Schematic illustration of the generation of hCRC organoid cultures from primary colon tumor samples (upper panel). IHC characterization of the primary tumor tissue (hCRC3 and 5) via H&E, Pan-CK and CDX2 staining (scale bars=100 µm). **(b)** Representative BF pictures (left panel), CK20 (middle panel) and CDX2 (right panel) IF staining of established tumoroid cultures (hCRC3, 5 and 7). Scale bars =100µm. **(c)** Exome sequencing analysis (Somatic Tumor Panel TUM01, CeGaT) of hCRC3, 5 and 7 tumoroid cultures.

3.11. Therapeutic potential of 1639 in human CRC cell lines and organoid cultures

The different mutational profiles of our three tumoroid cultures made them a suitable tool for a therapeutic validation of p38α inhibition in human CRC. To include even a broader spectrum of CRC genotypes the analysis was expanded to several well-established human CRC cell lines (HCT15, HT29 and HCT116). CTG viability assays were performed for all tested organoids (hCRC3, hCRC5 and hCRC7) and cell lines (HCT15, HT29 and HCT116). In all tested cultures a treatment with 1639 treatment lead to a strong therapeutic effect and a significantly higher induction of cell death in comparison to SKL (Fig. 13a, b). Of note, HCT15 seemed to be very sensitive regarding p38α inhibition in general, since even SKL induced a dose dependent reduction of cell viability.

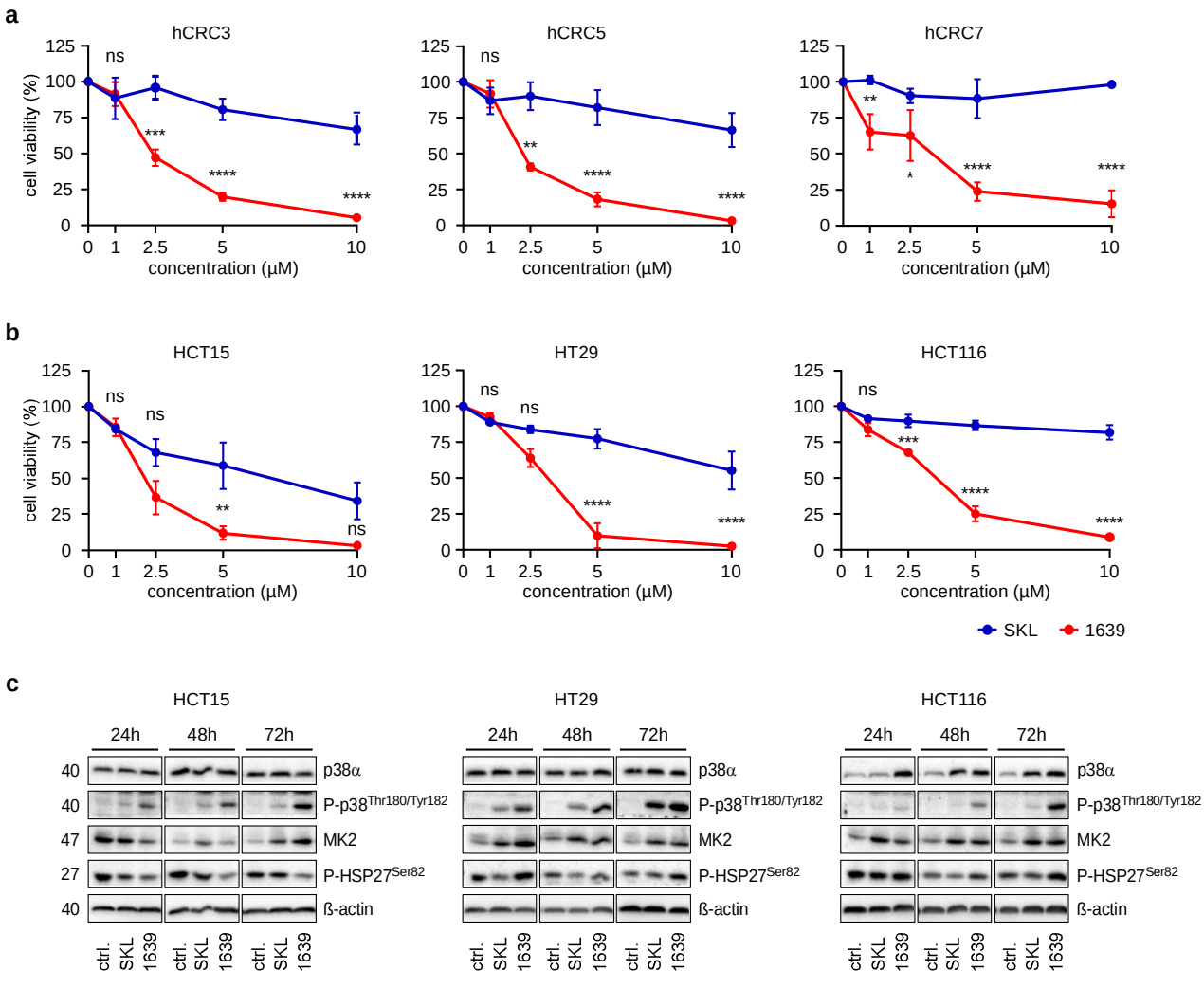

Figure 13. SKL and 1639 treatment of human CRC cell lines and organoids (a-b) Cell viability analysis using CTG of human tumoroid cultures **(a)** and CRC cell lines **(b)** treated with SKL or 1639 for four days. Cell viability was normalized to DMSO treated control. Statistical analysis: two-way ANOVA, Sidak's multiple comparisons test (SKL vs.1639). hCRC3 p-values from left: 0.9994 (ns), 0.0008 (***), <0.0001 (****). hCRC5 p-values from left: 0.9954 (ns), 0.0011 (**), <0.0001 (****). Data is depicted as mean with SD. n=3. (biological replicates). hCRC7 p-values from left: 0.0050 (**),0.0326 (*), <0.0001 (****). Data is depicted as mean with SD. n=2. (biological replicates). HCT15 p-values from left: >0.9999 (ns), 0.0801 (ns), 0.0041 (**), 0.0832 (ns). HT29 p-values from left: 0.9975 (ns), 0.1360 (ns), <0.0001 (****). HCT116 p-values from left: 0.4819 (ns), 0.0009 (***), <0.0001 (****).Data is depicted as mean with SD. n=3. (biological replicates). **(c)** Western blot analysis of total p38α, phosphorylated p38α and its downstream target HSP27 upon treatment with DMSO, SKL or 1639. Time course upon 24, 48 and 72 hours of treatment at a concentration of 1 µM (from left HCT15, HT29, HCT116 cells). β-actin was used as loading control.

In line with my previous data, I found increased phosphorylation level of p38 and an increase in total MK2 level upon 1639 treatment in HCT15, HT29 and HCT116 cells (72 hour time point). In contrast to the other two CRC cell lines, HT29 showed an initial downregulation of total MK2 and a sustained reduction of HSP27 phosphorylation upon 1639 treatment (Fig. 13c).

3.12. p38α kinase inhibitor drug screen in murine CRC organoids

My hitherto generated data revealed promising therapeutic effects of the p38α inhibitor 1639 in murine and human CRC cultures and well-established colon cancer cell lines. The fact that the selective p38α inhibitor SKL has only a very low effect on cell viability indicates that an optimized target residence time strongly increase the therapeutic potential of p38α inhibitors. However, also 1639 did not entirely block CRC development (especially in the CRC metastasis model).

1639 is part of the TüCAD2 compound library, a compound database comprising approximately 8500 compounds generated by the Laufer laboratory. A structure-based virtual screening approach identified 362 potential p38α inhibitors (*MAPK14* set) with varying target residence times (up to 5000 sec). All 362 compounds were ranked by their ability to block TNFα secretion in a whole-blood ELISA assay (Laufer lab). In order to identify even more potent therapeutic agents for the treatment of CRC the best 100 inhibitors (based on the TNFα ELISA) were selected for an organoid-based drug screen.

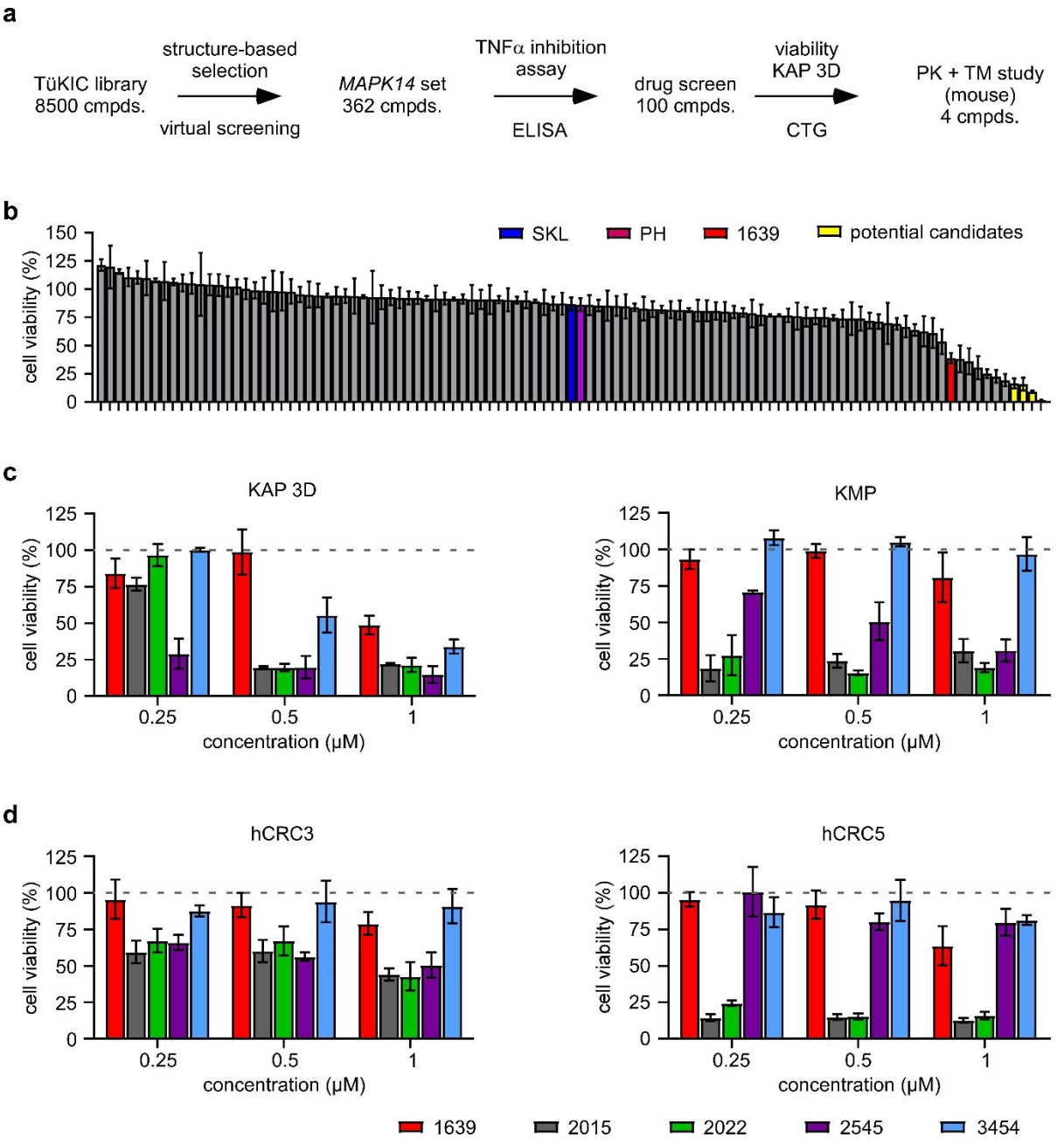

Figure 14. p38α inhibitor drug screen and potential candidate validation in murine and human CRC organoid cultures (a) schematic illustration of the p38α inhibitor screening for the selection of drug screen candidates. **(b)** p38α inhibitor drug screen with 100 novel compounds in KAP organoids. Cell viability analysis using CTG. Four days treatment at a concentration of 1 µM. Cell viability was normalized to DMSO treated control. Data is depicted as mean with SD. n=3. (biological replicates). **(c-d)** Validation of the potential candidates 2015, 2022, 2545, 3454 in comparison with 1639 using the CTG viability assay. The murine CRC organoid cultures KAP and KMP **(c)** and the human tumoroid cultures hCRC3 and hCRC5 **(d)** were treated for four days. Cell viability was normalized to DMSO treated control. Data is depicted as mean with SD. n=3. (biological replicates).

I applied the established murine KAP organoids to perform high-troughput CTG viability assays with the selected compound library (Fig. 14b, depicted in grey). SKL, PH and 1639 were included as controls. This drug screen, which was conducted over four days at a concentration of 1 µM, identified ten compounds that showed an even better therapeutic outcome than 1639. The Top 4 candidates (2015, 2022, 2545, 3454) were selected for further validation experiments (Fig. 14b, depicted in yellow). These candidates were tested in the murine CRC organoids KAP and KMP, as well as in the human CRC tumoroids hCRC3 and hCRC5. For cell viability analysis, CTG assays were performed with a treatment duration of four days and a concentration series ranging from 0.25 to 1 µM (Fig. 14c, d). These assays revealed a pronounced therapeutic effect of 2015 and 2022 in all tested cultures that was superior to the therapeutic effect of 1639 (Fig. 14 c, d). While a 0.5 µM concentration reduced the cell viability to below 25% in KAP, KMP and hCRC5 cells, hCRC3 seemed to be in general less sensitive to p38α inhibition.

In line with my hypothesis that the target residence time of p38α inhibitors influences the treatment response in CRC, 2015 showed a target residence time of 5256 seconds. These results indicate that new generation p38α inhibitors with strongly increased target residence times can further improve the therapeutic effect of p38α inhibition in colorectal cancer.

4. Discussion and outlook

Each year nearly 900.000 people die of CRC, which accounts for approximately 10% of all cancer related deaths worldwide [1]. Therapeutic options for patients with advanced metastasized (stage IV) CRC are still limited. Recent therapies that combine Oxaliplatin- and Irinotecan-based chemotherapies with monoclonal antibodies against VEGFR or EGFR prolong survival of stage IV CRC patient by only two years in average [99]. Importantly, also immunotherapies based on checkpoint blocking antibodies like anti-PD1 or anti-CTLA4, which allow for long term tumor control in different tumor entities such as lung cancer and melanoma [100], show only limited activity in CRC. Only microsatellite instable CRC, which account for less than 3% of all CRC seem to respond to checkpoint blocking antibodies. Therefore, novel therapeutic options for colorectal cancer patients are urgently needed.

In order to improve the outcome for CRC patients, clinical cancer research has focused on the identification of new treatment strategies for many years. Multidisciplinary approaches have led to the generation and validation of new therapeutic agents for cancer therapy. However, not even 10% of drugs that entered clinical trials were approved by the authorities in the last 20 years [101]. Closing the gap between biomedical research and the applicability at the bedside has therefore been referred to as “crossing the valley of death” [102]. A major limitation of translational cancer research is the lack of physiological models which reflect the human disease in order to provide data that can be translated into the clinic easier. This also accounts for colorectal cancer research.

It was recently shown that p38α represents an important factor in the development of colorectal cancer [29]. However, these data were achieved in a mouse model of colitis induced colorectal cancer and colitis-associated cancer (CAC) represents only 1 to 2% of all CRC cases [9]. This is one of the major disadvantages of mouse models using carcinogens for the induction of CRC. In addition, the tumorigenesis has been described as difficult to reproduce, since the susceptibility to carcinogens such as DSS or AOM varies depending on the mouse strain [103, 104]. Although the chemically induced carcinogenesis accompanied mutational profile has been proven

to accurately resemble CAC [105], the model is rather inadequate for investigating the treatment response of colitis-independent CRC.

With the aim to address the role of p38α inhibition in colitis independent CRC, I established murine colon- and patient-derived tumor organoid cultures in this study. By using GEMMs and CRISPR/Cas9 technology, murine colon organoids were first isolated and then transformed *in vitro.* 3D CRC organoid cultures are described to represent physiological tools for translational research, e.g. due to the fact that the tumor heterogeneity is maintained [57, 58, 82]. It could already been demonstrated, that 3D cultures show a different treatment response in comparison to 2D cell lines indicating that the data obtained from organoid-based drug screens delivers a much more adequate representation of the treatment response in cancer patients [106, 107]. Highlighting the importance of intra-tumor heterogeneity, Ben-David et al. demonstrated that the 2D culture condition favors the outgrowth of highly proliferative clones, thereby leading to clonal evolution. Their study revealed that the drug treatment response is greatly altered due to this genetic instability, thus proving that clonal evolution has a major influence on reproducibility [108]. The maintenance of intra-tumor heterogeneity and increased translational potential of organoids is achieved by culture conditions including an extracellular scaffold and a cocktail of universal and tissue-specific growth factors. In contrast to common 2D culture media, which rarely differ for the variety of existing cancer cells, organoid media are highly specialized. The composition greatly depends on the originating tissue of the established culture. The complex organoid culture conditions hereby aim to mimic the tumor microenvironment. The generation of organoid media involves the use of tissue-specific growth factors and varies for freshly isolated tissue or already established cultures. Furthermore, depending on the molecular profile of the tumor tissue, media and culture conditions (e.g. oxygen levels, scaffolds) are adapted to provide more physiological microenvironments [63]. Some of the more frequently studied examples are the dependence of *APC* WT CRC organoids on the recombinant protein Wnt3a or the influence of *RAS* and *RAF* mutations on EGF necessity. Of note, the ability of tumor organoid cultures to steadily grow even without being given certain media components represents a great advantage regarding selection of specific genotypes. This genotype specific loss of growth factor dependencies allowed us to differentiate between healthy and transformed organoids in this study.

Recent efforts to improve and adapt culture conditions strongly increased the success rates for establishing organoids from patient material. In contrast, it remains difficult to generate patient-derived 2D cultures which grow steadily in culture. Drexler et al. attribute this low success rate to the harsh changes in the microenvironment when taking tumor material into culture [109]. Especially for CRC organoids high success rates for the generation of cultures from tumor biopsies have been reported [63, 82, 110]. Although organoid cultures were shown to be genetically stable, a recent study analyzing 55 CRC derived organoids found out that MSI lines acquire new mutations correlating with prolonged culture duration [63]. On one hand, this highlights the need to keep track of passage numbers and to verify the mutational profile over time; on the other hand, this offers an opportunity to investigate molecular changes during treatment in order to analyze mechanisms of acquired therapy resistance.

I analyzed the expression of common colon epithelial markers in the generated cultures and found their expression to be maintained upon transformation to CRC. The mutational profile was confirmed by genetic analyses, although KAP organoids were not tested for additional mutations and clonality. Since the transfection efficacy was at approximately 10% and several studies published the maintenance of heterogeneity in organoid cultures it is unlikely that KAP organoids were established from only a few clones. However, it could be possible that the 2D culture of KAP organoids favored clonal evolution. No loss of differentiation was detected during culturing and subcutaneous injection of KAP 3D cells resulted in the outgrowth of moderately differentiated tumors.

The histological characterization of CRC tumor tissue is based on the percentage of glandular formation. In well differentiated CRC over 95% of the tumor tissue is composed of glandular structures, whereas glands only account for 50-95% in moderately differentiated tumors. This common approach is also used in the clinic in order to evaluate tumor grading. Most CRC patients are diagnosed with moderately differentiated tumor tissue (70%); well differentiated tumors occur in 10% of the adenocarcinoma cases. A poor differentiation of the tumor, characterized by less than 50% of gland formation, is observed in 20% of the CRC patients [111]. To our practical knowledge, the subcutaneous injection of traditional cancer cell lines rarely resulted in the formation of differentiated tumor tissue in the past.

To reduce the risk of genetic alteration, KAP 2D and 3D cultures were always used at early passages for every experiment conducted in this study. Nonetheless, a more detailed analysis including DNA, protein and mRNA expression profiles as well as epigenetic modifications could be performed in the future in order to accurately compare KAP 3D organoids over time and to compare KAP 3D with 2D cultures.

The subcutaneous and splenic injection of KAP organoids into mice resulted in the outgrowth of moderately differentiated tumors, regardless of the mouse genotype. A solid tumor and a liver metastases model were established, which allow to efficiently mimic the human disease. Nevertheless, a model of a constantly progressing disease with a primary tumor in the colon that metastasizes via the portal vein into the liver would be eligible. Such a model would allow for investigating cancer metastases under physiological conditions and yield significant translational impact.

Recently, O'Rourke et al. were able to transplant CRC organoids into the colon of mice and could show that arising primary tumors progressed into an advanced metastatic disease (depending on the mutational profile). However, the percentage of successfully engrafted tumors was low and tumor development was only achieved by DSS-induced tissue damage of the intestinal mucosa [83]. DSS exposure leads to massive inflammation, wound bed formation in the epithelium and thereby increasing the probability of engraftment. Therefore, these tumors do not actually represent colitis-independent CRCs. Nevertheless, the model of O'Rourke et al. represents a promising tool to study the treatment response of colon tumors and it would be interesting to take advantage of this combined inflammation and CRC model in the future. Since CRC development spans over several years and a sequential mutagenesis is observed in 70-90% of all CRC cases it would be interesting to investigate therapeutic options in different stages of the disease. Furthermore, the influence of tumor evolution and clonal resistance in progressing cancerous lesions should be taken into consideration when investigating new treatment strategies.

Gupta et al. characterized ablation of the p38α gene *Mapk14* in CAC by using a tamoxifen-inducible knockout mouse model [29]. In my study, the effect of genetic *Mapk14* attenuation in colitis-independent CRC was studied using shRNA-mediated gene knockdown. Importantly, I found that blockade of *Mapk14* also affected the cell viability of colitis independent CRCs. Interestingly, the knockdown efficiency varied

between the six tested shRNAs and the knockdown efficiency was correlated with the treatment response. Since the p38α gene *Mapk14* could be proven to be an important factor for the maintenance of both, colitis-induced and colitis-independent CRC, I thought to establish a therapy that is based on pharmacological p38α inhibition. However, established and highly selective p38α inhibitors (Skepinone-L (SKL) [85], PH797804 [86]) showed only very weak therapeutic effects in organoids and CRC cells *in vitro* and no therapeutic effects in murine CRC in *vivo*. These data reveal that target identification using genetic assays do not automatically pave the way for a pharmacological treatment strategy.

Other studies also identified p38α as a valuable target in CRC therapy and it has been shown that p38α inhibition sensitizes CRC cancer cells towards chemotherapy [40, 112, 113]. Similar to our results striking effects on cell viability are rarely seen with current p38α inhibitors when given as a monotherapy *in vitro*. Of note, in the case of the combined p38α/β inhibitor SB203580 high concentrations are necessary to induce cell death when administered as a single agent. Comparable with our results, SB203580-mediated p38α inhibition results in caspase activation and cell death. However, to achieve potent induction of apoptosis the combination with 5'FU was necessary [113]. *In vivo*, the selective p38α inhibitor PH797804 has been shown to slightly reduce the tumor burden in PDX models of CRC [114], but little is known about the treatment response towards Skepinone-L when given as a monotherapy. However, a promising therapeutic outcome was reported in a combinational therapy with the multi-kinase inhibitor Sorafenib in a mouse model of HCC [39]. Hence, selectivity can be considered as a promising start to improve treatment options for patients but other aspects of drug target interaction need to be addressed as well. This hypothesis is further supported by our results showing striking difference between pharmacological inhibition of a target and genetic inhibition of the corresponding gene.

Of note, the mode of action strongly differs between gene specific mRNA destruction and pharmacological protein inhibition. In order to understand, why a pharmacological inhibition of p38α with established compounds is less effective than a genetic inhibition of the p38α gene *Mapk14*, I analyzed the expression and activity of p38α during treatment. Interestingly, increased phosphorylation of p38 and increased activity of the p38α downstream target MK2 were detected upon treatment with the p38α inhibitors. My current data indicates that p38α inhibition triggers a

paradoxically activation of p38α which impedes further inhibition of this target. Thus, it seems that very pronounced pharmacological inhibition of p38α is needed to phenocopy a genetic knockdown of *Mapk14*. Of note, no isoform-specific antibody for the detection of the phosphorylated state of p38α exists and a more detailed investigation of changes in protein expression and phosphorylation will be insightful in the future.

With regard to the drug-target dissociation constant it has been described that increasing inhibitor concentrations lead to prolonged drug-target interaction. This dynamic reaction mainly depends on the binding affinity of the inhibitor and the saturation of the system [115, 116]. However, the ambition to achieve a more efficacious saturation by increasing drug concentrations is limited by the inhibitor affinity towards other targets. To avoid off-target effects and still improve inhibitor-target engagement prolonged target residence times represent a valuable option, since the duration of the interaction is taken more into account than the solemn binding affinity of a given inhibitor-target complex [117]. This approach thereby reduces the risk of off-target effects, making it easier to study target-specific interactions and to avoid adverse events.

In order to investigate if target residence times play a role regarding the potency of p38α inhibitors, I next applied the p38α inhibitor LN1639 for further analysis. LN1639 represents a selective type 1.5 p38α inhibitor with an optimized target residence time and a kinetic that is comparable to SKL (data from AG Laufer). In comparison to SKL, the inhibitor-kinase interaction of LN1639 was improved to 259 seconds. Importantly, in contrast to Type II inhibitors such as BIRB-796 which also show a long target residence time, Type 1.5 inhibitors are able to bind to the active and inactive protein and show a higher specificity to p38α than Type II inhibitors. Indeed, improved therapeutic efficacy was observed upon treatment of CRC with LN1639 *in vitro* and *in vivo*. Significant cell death induction (CTG) and delayed subcutaneous tumor growth were detected upon LN1639 treatment. *In vitro,* an effect of LN1639 on cell viability was observed following 24 hours of treatment and an EdU incorporation assay revealed significantly decreased proliferation at the 24 hour time point. The recently developed p38α inhibitor LN1639 belongs to a distinct class of kinase inhibitors. In comparison to SKL, a classical type I inhibitor, the binding of LN1639 does not occur in a fully ATP-competitive mode of action. The interaction of the type 1.5 inhibitors, such as LN1639, is based on the engagement of the R-spine and additional binding

to the DFG-motif of the kinase. Binding to the R-spine can occur in the active as well as in the inactive state of the kinase, an important factor regarding inhibitor-enzyme engagement. Therefore, this approach has led to the development of highly selective p38α inhibitors with improved target residence times and picomolar activity on the enzyme itself [118]. My data demonstrate that the improved binding of LN1639 results in increased potency. In addition, our results strongly indicate that optimized type 1.5 inhibitors with increased target residence time are able to inhibit targets that are strongly expressed or activated in cancer cells. Furthermore, such inhibitors might be useful to block the development of secondary therapy resistance.

Of note, in the CRC metastasis model, two mice did not respond to the treatment with the optimized p38α inhibitor LN1639. However, the statistical analysis revealed a tendency towards prolonged survival in LN1639 treated mice (p-value=0.1623). This result indicates that compounds with further increased target residence time may also further improve the therapeutic efficacy of p38α inhibition. Thus, I performed a compound screen in CRC organoids (KAP 3D) with 100 additional p38α inhibitors with varying target residence times. This p38α inhibitor drug screen identified several new p38α inhibitors with a much higher therapeutic efficacy than LN1639 in different murine and human CRC cultures (e.g. LN2015) The target residence time of our top candidate LN2015 accounts for 5256 seconds, further exceeding the target residence time of LN1639. These results further emphasize the effect of optimized target inhibitor engagement for the therapeutic efficacy of p38α inhibitors in CRC. Since LN2015 showed also high plasma levels and metabolic stability in mice (data from AG Laufer), this compound may have a great potential for the treatment of cancer patients in the future. Of note, the therapeutic potential of this compound needs to be thoroughly tested in different CRC mouse models *in vivo.*

Since already LN1639 showed striking effects *in vitro* and *in vivo,* this inhibitor was expected to drastically downregulate p38α downstream targets. Thus, the observed activation of MK2 and ATF2 was surprising. Only the phosphorylation of HSP27 seemed to be blocked upon SKL and LN1639 treatment in KAP 2D cells. Interestingly, the western blot analysis of LN1639 treated cells revealed a significantly stronger activation of p38α and p38α downstream signaling in comparison to SKL, even though apoptosis induction could clearly be detected by

accumulation of cleaved caspase 3. On the one hand the increased phosphorylation of p38 and its downstream targets seems contradictory on the other hand it is well known that p38α signaling is linked to the cellular stress response. The chosen concentration of 1 µM leads to a reduction in cell viability of approximately 50% in KAP 2D cells (4 days of treatment). The remaining cells, which were used for the analysis, might be stimulated in a paracrine mode of action by the dying cells. In order to analyze whether there is a paracrine activation of p38α during treatment, an experiment with conditioned medium was performed. The conditioned medium was produced by treating KAP 2D cells with 1 µM SKL or LN1639 and compared to a DMSO treated control. Following the treatment of four hours, cells were washed to remove the inhibitors and left for additional four hours in compound-free medium. The conditioned medium strongly induced p38α activation and even the producing cells remained in the activated state after four hours of treatment withdrawal supporting the hypothesis of a paracrine signal transduction.

Upon stimulation, p38α is known to lead to the production of pro-inflammatory cytokines with TNFα being the most prominent one. The defects in TNFα translation obtained in the MK2 knockout mouse confirm the connection between the p38α signaling pathway and the pro-inflammatory cytokine [119]. Furthermore, it was shown that p38α activation leads to the stabilization of *Tnfα* mRNA [120]. TNFα itself can then stimulate the MAPK pathway, including p38α, in a positive feedback mechanism [28, 89, 121]. In line with those findings, the incubation of KAP 2D cells with recombinant TNFα led to an induction of p38α comparable with SKL treatment. Interestingly, I found increased secretion of TNFα in LN1639 treated cells in an ELISA assay. Furthermore, an induction of TNFα mRNA was detected by RT-qPCR analysis in LN1639 treated KAP 2D cells (5 µM concentration) and in cells with stable, shRNA-mediated knockdown of *Mapk14*, indicating that activation and increased secretion of TNFα is involved in the paradoxically activation of p38α under treatment.

Since TNFα is known to induce apoptosis in certain cell types [122] and reported to possess a dual role in breast cancer [123], I also analyzed the effect of the pro-inflammatory cytokine on cell viability. The additional elevation of TNFα levels by using recombinant protein only resulted in a minimal decrease of viable cells, even

when using the doxycycline induced sh2605 cell line. Thus, the performed experiments indicate that the secretion of TNFα is not critical for the treatment response. Since, TNFα is not the only cytokine affected by p38α, I also focused on IL6 and STAT3, two key mediators of the p38α-mediated pro-inflammatory cytokine signature. It has been shown that p38α inhibition in murine CAC results in lower *Il6* mRNA levels and reduced phosphorylation of STAT3 [29]. In addition, the activation of the Nf-κB pathway was analyzed since it is intertwined with both, the p38α and the TNFα signaling cascades. Furthermore, Nf-κB activation is commonly detected following p38α induction [29] and has been linked to intestinal tumorigenesis [124]. Fitting to the hypothesis that p38α activation is stimulated in a paracrine way of action in order to cope with stress induced by p38α inhibition, increased *Il6* mRNA levels and Nf-κB signaling was detected. Nf-κB activation was hereby determined by measuring mRNA levels of the inhibitory unit *Nfkbia*. The induction of *Nfkbia* can directly be correlated to Nf-κB pathway induction. STAT3 mRNA levels remained stable upon p38α inhibitor treatment or shRNA-mediated knockdown of *Mapk14*, indicating that the transcription factor is not essential for the treatment-induced stress response. Nonetheless, the analysis needs to be expanded in the future in order to obtain a complete secretory profile and also other regulatory mechanisms (e.g. post-transcriptional modifications) need to be considered.

It has been shown that p38α can mediate a cell cycle arrest in G2/M through the phosphorylation of the phosphatase Cdc25c and Cdc25B following UV radiation. The inhibition of Cdc25 causes CDK1 inhibition and thereby a delay in G2/M transition [125]. In line with these results, we observed that LN1639 treatment leads to decreased CDK1 phosphorylation and thereby potentially causes an accelerated cell cycle progression. In line with this, we found lower Cyclin B1 levels and a reduced G2/M phase in LN1639 treated cells. The detected increase in the subG1 population indicates that p38α inhibition affects cell viability. Since it is a well-known fact that an impaired G2/M checkpoint induces DNA damage also the phosphorylation status of histone H2AX was analyzed [127]. Indeed, LN1639 treatment of KAP 2D cells resulted in a strong induction of DNA damage and cell death in a dose-dependent manner. Therefore, LN1639 was compared to DNA damage inducing chemotherapeutic agents. Platinum-based chemotherapy is a standard treatment option for CRC patients suffering from advanced disease. The comparison of the treatment response of LN1639 with chemotherapy resulted in striking differences

regarding potency. KAP 2D and 3D cultures were more sensitive towards p38α inhibition than 5'FU, Irinotecan and Oxaliplatin. This might be due to the combination of disrupted stress signaling and induction of DNA damage. The therapeutic benefit of combining p38α inhibition with Irinotecan or Cisplatin treatment has already been demonstrated in CRC studies, but so far with less potent p38α inhibitors than LN1639 [40, 41]. The optimization of target residences times could therefore further increase the combinatorial effect.

Taken together this study demonstrates that the therapeutic value of p38α inhibition in CRC is greatly influenced by target-inhibitor interaction. Hence, I was able to prove that the optimization of target residence time is essential for improved therapeutic efficacy.

The first generation p38α inhibitor LY2228820 has already shown some promising effects in a fraction of patients with advanced cancer. However, only 21% of the enrolled patients achieved stable disease with a median duration of 3.7 months [128]. In a study in ovarian cancer, the combination of LY2228820 and gemcitabine resulted in modest improvement of progression free survival when compared to chemotherapy alone [129]. A phase I study of the p38α inhibitor LY3007113 in patients with advanced cancer had to be terminated due to toxicity concerns. Only 3 out of 27 presented with stable disease and a sustained biologically effective dose could not be achieved [130]. However, due to limited target-inhibitor interaction high concentrations of the compound are needed in order to effectively inhibit p38α kinase activity. The optimized target residence time of the type 1.5 p38α inhibitors presented within this study might result in a more favorable outcome regarding toxicity and overall survival since high selectivity can be achieved with lower concentrations. Since a cohort of patients with advanced cancer benefited from LY2228820 treatment in past clinical trials, we strongly believe that prolonged p38α inhibition will result in increased tolerability and progression free survival. Therefore, the evaluation of the novel p38α inhibitors presented within this study harbors the potential to provide a powerful therapy for patients suffering from advanced CRC.

5. Acknowledgement

First of all, I would like to thank my supervisor and mentor, Professor Stefan Laufer. Without his knowledge and experience in the field of pharmaceutical chemistry and of course his striking compound library this project would not have been possible. I am very grateful for the insightful meetings and the fruitful collaboration with his research group. A special thank you goes to Michael Forster, Mark Kudolo and Vanessa Haller for the development and testing of the p38α inhibitors.

I also would like to thank my second supervisor Professor Lars Zender, whose expertise was invaluable. Furthermore, thanks to his and Dr. Daniel Dauchs effort, I was able to acquire the necessary technical knowledge of establishing organoid cultures, an essential skill for conducting this thesis.

Of course, I want to thank the leader of the research group, Dr. Daniel Dauch, who guided me in formulating the research questions and methodology. He was my direct and daily supervisor and the intense discussions helped me to further improve my scientific thinking. In my time as a PhD student in his research group I gained valuable skills, not only for completing my thesis but also for my future.

I am grateful for the help, support and skills of all people involved in the p38α project. I would like to acknowledge Professor Ulrich Rothbauer, whose critical thinking and highly organized research methods impressed me a lot, as well as Dr. Philipp Kaiser for sharing and discussing their data with me. I would like to thank Dr. Tatu Pantsar for the virtual modelling and feedback on drug-target interaction and Dr. Thales Kroneberger for his biostatistical analysis of the patient data. For their effort to provide me with patient-derived tumor material and managing the logistics behind it I would like to thank Professor Alfred Königsrainer, Professor Ulrich Lauer, Professor Michael Bitzer and Dr. Can Yurttas, as well as the pathology team.

In addition I want to thank Dr. Ramona Rudalska, Agata Dylawerska and Aylin Heinrich for their help and support in our small research group. I have fond memories of all of them and enjoyed working with them.

I would like to acknowledge all of my former colleagues for 4 ½ years of wonderful collaboration. I would like to thank Pearl Schiemann and Lea Hermann for all of their work “behind the scenes”, without them the lab could not run so smoothly. I want to single out Elke Rist, Dr. Marco Seehawer, Dr. Sabrina Klotz and Melanie Henning for their technical support, assistance, scientific feedback and especially for their friendship, which helped me through the challenging moments of the PhD thesis.

Last but not least I want to thank my husband, his family and my own family who always supported and believed in me. They provided me with guidance and showed immense understanding for my limited time. When I was down they put me back up on my feet and set my head straight.

Throughout the whole project I have received great guidance, support and assistance from all those people and I am very grateful for it. Thank you all, without you I could not have done it.

6. References

1. Bray, F., et al., *Global cancer statistics 2018: GLOBOCAN estimates of incidence and mortality worldwide for 36 cancers in 185 countries.* CA Cancer J Clin, 2018. **68**(6): p. 394-424.
2. Howlader, N., et al., *SEER Cancer Statistics Review, 1975-2017, National Cancer Institute.* Based on November 2019 SEER data submission.
3. Aleksandrova, K., et al., *Combined impact of healthy lifestyle factors on colorectal cancer: a large European cohort study.* BMC Med, 2014. **12**: p. 168.
4. Henrikson, N.B., et al., *Family history and the natural history of colorectal cancer: systematic review.* Genet Med, 2015. **17**(9): p. 702-12.
5. Dekker, E., et al., *Colorectal cancer.* Lancet, 2019. **394**(10207): p. 1467-1480.
6. Kastrinos, F. and S. Syngal, *Inherited colorectal cancer syndromes.* Cancer J, 2011. **17**(6): p. 405-15.
7. Cancer Genome Atlas, N., *Comprehensive molecular characterization of human colon and rectal cancer.* Nature, 2012. **487**(7407): p. 330-7.
8. Gonzalez, R.S., K. Washington, and C. Shi, *Current applications of molecular pathology in colorectal carcinoma.* Applied Cancer Research, 2017. **37**(1): p. 13.
9. Munkholm, P., *Review article: the incidence and prevalence of colorectal cancer in inflammatory bowel disease.* Aliment Pharmacol Ther, 2003. **18 Suppl 2**: p. 1-5.
10. Lakatos, P.L. and L. Lakatos, *Risk for colorectal cancer in ulcerative colitis: changes, causes and management strategies.* World J Gastroenterol, 2008. **14**(25): p. 3937-47.
11. Terzic, J., et al., *Inflammation and colon cancer.* Gastroenterology, 2010. **138**(6): p. 2101-2114 e5.
12. Grady, W.M. and C.C. Pritchard, *Molecular alterations and biomarkers in colorectal cancer.* Toxicol Pathol, 2014. **42**(1): p. 124-39.
13. Kuipers, E.J., et al., *Colorectal cancer.* Nat Rev Dis Primers, 2015. **1**: p. 15065.
14. Valori, R., et al., *European guidelines for quality assurance in colorectal cancer screening and diagnosis. First Edition--Quality assurance in endoscopy in colorectal cancer screening and diagnosis.* Endoscopy, 2012. **44 Suppl 3**: p. SE88-105.
15. Sauer, R., et al., *Preoperative versus postoperative chemoradiotherapy for locally advanced rectal cancer: results of the German CAO/ARO/AIO-94 randomized phase III trial after a median follow-up of 11 years.* J Clin Oncol, 2012. **30**(16): p. 1926-33.
16. van Gijn, W., et al., *Preoperative radiotherapy combined with total mesorectal excision for resectable rectal cancer: 12-year follow-up of the multicentre, randomised controlled TME trial.* Lancet Oncol, 2011. **12**(6): p. 575-82.
17. Labianca, R., et al., *Early colon cancer: ESMO Clinical Practice Guidelines for diagnosis, treatment and follow-up.* Ann Oncol, 2013. **24 Suppl 6**: p. vi64-72.
18. Van Cutsem, E., et al., *Metastatic colorectal cancer: ESMO Clinical Practice Guidelines for diagnosis, treatment and follow-up.* Ann Oncol, 2014. **25 Suppl 3**: p. iii1-9.
19. Ikoma, N., K. Raghav, and G. Chang, *An Update on Randomized Clinical Trials in Metastatic Colorectal Carcinoma.* Surg Oncol Clin N Am, 2017. **26**(4): p. 667-687.

20. Spano, J.P., et al., *Impact of EGFR expression on colorectal cancer patient prognosis and survival.* Ann Oncol, 2005. **16**(1): p. 102-8.

21. Douillard, J.Y., et al., *Panitumumab-FOLFOX4 treatment and RAS mutations in colorectal cancer.* N Engl J Med, 2013. **369**(11): p. 1023-34.

22. Hurwitz, H., et al., *Bevacizumab plus irinotecan, fluorouracil, and leucovorin for metastatic colorectal cancer.* N Engl J Med, 2004. **350**(23): p. 2335-42.

23. Van Cutsem, E., et al., *Addition of aflibercept to fluorouracil, leucovorin, and irinotecan improves survival in a phase III randomized trial in patients with metastatic colorectal cancer previously treated with an oxaliplatin-based regimen.* J Clin Oncol, 2012. **30**(28): p. 3499-506.

24. Overman, M.J., et al., *Durable Clinical Benefit With Nivolumab Plus Ipilimumab in DNA Mismatch Repair-Deficient/Microsatellite Instability-High Metastatic Colorectal Cancer.* J Clin Oncol, 2018. **36**(8): p. 773-779.

25. Koopman, M., et al., *Deficient mismatch repair system in patients with sporadic advanced colorectal cancer.* Br J Cancer, 2009. **100**(2): p. 266-73.

26. Cuenda, A. and S. Rousseau, *p38 MAP-kinases pathway regulation, function and role in human diseases.* Biochim Biophys Acta, 2007. **1773**(8): p. 1358-75.

27. Cuadrado, A. and A.R. Nebreda, *Mechanisms and functions of p38 MAPK signalling.* Biochem J, 2010. **429**(3): p. 403-17.

28. Zarubin, T. and J. Han, *Activation and signaling of the p38 MAP kinase pathway.* Cell Res, 2005. **15**(1): p. 11-8.

29. Gupta, J., et al., *Dual function of p38alpha MAPK in colon cancer: suppression of colitis-associated tumor initiation but requirement for cancer cell survival.* Cancer Cell, 2014. **25**(4): p. 484-500.

30. Bulavin, D.V., et al., *Inactivation of the Wip1 phosphatase inhibits mammary tumorigenesis through p38 MAPK-mediated activation of the p16(Ink4a)-p19(Arf) pathway.* Nat Genet, 2004. **36**(4): p. 343-50.

31. Chen, L., et al., *Inhibition of the p38 kinase suppresses the proliferation of human ER-negative breast cancer cells.* Cancer Res, 2009. **69**(23): p. 8853-61.

32. Ventura, J.J., et al., *p38alpha MAP kinase is essential in lung stem and progenitor cell proliferation and differentiation.* Nat Genet, 2007. **39**(6): p. 750-8.

33. Hui, L., et al., *p38alpha suppresses normal and cancer cell proliferation by antagonizing the JNK-c-Jun pathway.* Nat Genet, 2007. **39**(6): p. 741-9.

34. Yang, L., et al., *p38alpha Mitogen-Activated Protein Kinase Is a Druggable Target in Pancreatic Adenocarcinoma.* Front Oncol, 2019. **9**: p. 1294.

35. Wang, S.N., et al., *Phosphorylated p38 and JNK MAPK proteins in hepatocellular carcinoma.* Eur J Clin Invest, 2012. **42**(12): p. 1295-301.

36. Greenberg, A.K., et al., *Selective p38 activation in human non-small cell lung cancer.* Am J Respir Cell Mol Biol, 2002. **26**(5): p. 558-64.

37. Esteva, F.J., et al., *Prognostic significance of phosphorylated P38 mitogen-activated protein kinase and HER-2 expression in lymph node-positive breast carcinoma.* Cancer, 2004. **100**(3): p. 499-506.

38. Cheng, Y., et al., *p38 predicts depression and poor outcome in esophageal cancer.* Oncol Lett, 2017. **14**(6): p. 7241-7249.

39. Rudalska, R., et al., *In vivo RNAi screening identifies a mechanism of sorafenib resistance in liver cancer.* Nat Med, 2014. **20**(10): p. 1138-46.

40. Paillas, S., et al., *Targeting the p38 MAPK pathway inhibits irinotecan resistance in colon adenocarcinoma.* Cancer Res, 2011. **71**(3): p. 1041-9.

41. Germani, A., et al., *Targeted therapy against chemoresistant colorectal cancers: Inhibition of p38alpha modulates the effect of cisplatin in vitro and in vivo through the tumor suppressor FoxO3A.* Cancer Lett, 2014. **344**(1): p. 110-118.

42. Barker, N., et al., *Identification of stem cells in small intestine and colon by marker gene Lgr5.* Nature, 2007. **449**(7165): p. 1003-7.

43. Sato, T., et al., *Single Lgr5 stem cells build crypt-villus structures in vitro without a mesenchymal niche.* Nature, 2009. **459**(7244): p. 262-5.

44. O'Rourke, K.P., et al., *Isolation, Culture, and Maintenance of Mouse Intestinal Stem Cells.* Bio Protoc, 2016. **6**(4).

45. Rock, J.R., et al., *Basal cells as stem cells of the mouse trachea and human airway epithelium.* Proc Natl Acad Sci U S A, 2009. **106**(31): p. 12771-5.

46. Huch, M., et al., *Long-term culture of genome-stable bipotent stem cells from adult human liver.* Cell, 2015. **160**(1-2): p. 299-312.

47. Boj, S.F., et al., *Organoid models of human and mouse ductal pancreatic cancer.* Cell, 2015. **160**(1-2): p. 324-38.

48. Sato, T., et al., *Long-term expansion of epithelial organoids from human colon, adenoma, adenocarcinoma, and Barrett's epithelium.* Gastroenterology, 2011. **141**(5): p. 1762-72.

49. Bartfeld, S., et al., *In vitro expansion of human gastric epithelial stem cells and their responses to bacterial infection.* Gastroenterology, 2015. **148**(1): p. 126-136 e6.

50. Chua, C.W., et al., *Single luminal epithelial progenitors can generate prostate organoids in culture.* Nat Cell Biol, 2014. **16**(10): p. 951-61, 1-4.

51. Karthaus, W.R., et al., *Identification of multipotent luminal progenitor cells in human prostate organoid cultures.* Cell, 2014. **159**(1): p. 163-175.

52. DeWard, A.D., J. Cramer, and E. Lagasse, *Cellular heterogeneity in the mouse esophagus implicates the presence of a nonquiescent epithelial stem cell population.* Cell Rep, 2014. **9**(2): p. 701-11.

53. Sachs, N., et al., *A Living Biobank of Breast Cancer Organoids Captures Disease Heterogeneity.* Cell, 2018. **172**(1-2): p. 373-386 e10.

54. Grassi, L., et al., *Organoids as a new model for improving regenerative medicine and cancer personalized therapy in renal diseases.* Cell Death Dis, 2019. **10**(3): p. 201.

55. Sakaguchi, H., et al., *Generation of functional hippocampal neurons from self-organizing human embryonic stem cell-derived dorsomedial telencephalic tissue.* Nat Commun, 2015. **6**: p. 8896.

56. Lancaster, M.A., et al., *Cerebral organoids model human brain development and microcephaly.* Nature, 2013. **501**(7467): p. 373-9.

57. van de Wetering, M., et al., *Prospective derivation of a living organoid biobank of colorectal cancer patients.* Cell, 2015. **161**(4): p. 933-45.

58. Huang, L., et al., *Ductal pancreatic cancer modeling and drug screening using human pluripotent stem cell- and patient-derived tumor organoids.* Nat Med, 2015. **21**(11): p. 1364-71.

59. Broutier, L., et al., *Human primary liver cancer-derived organoid cultures for disease modeling and drug screening.* Nat Med, 2017. **23**(12): p. 1424-1435.

60. Batchelder, C.A., et al., *Three Dimensional Culture of Human Renal Cell Carcinoma Organoids.* PLoS One, 2015. **10**(8): p. e0136758.

61. Lee, S.H., et al., *Tumor Evolution and Drug Response in Patient-Derived Organoid Models of Bladder Cancer.* Cell, 2018. **173**(2): p. 515-528 e17.

62. Kopper, O., et al., *An organoid platform for ovarian cancer captures intra- and interpatient heterogeneity.* Nat Med, 2019. **25**(5): p. 838-849.

63. Fujii, M., et al., *A Colorectal Tumor Organoid Library Demonstrates Progressive Loss of Niche Factor Requirements during Tumorigenesis.* Cell Stem Cell, 2016. **18**(6): p. 827-38.

64. Verissimo, C.S., et al., *Targeting mutant RAS in patient-derived colorectal cancer organoids by combinatorial drug screening.* Elife, 2016. **5**.

65. Porotto, M., et al., *Authentic Modeling of Human Respiratory Virus Infection in Human Pluripotent Stem Cell-Derived Lung Organoids.* mBio, 2019. **10**(3).

66. Nakamura, T., *Recent progress in organoid culture to model intestinal epithelial barrier functions.* Int Immunol, 2019. **31**(1): p. 13-21.

67. Schwank, G., et al., *Functional repair of CFTR by CRISPR/Cas9 in intestinal stem cell organoids of cystic fibrosis patients.* Cell Stem Cell, 2013. **13**(6): p. 653-8.

68. Andersson-Rolf, A., et al., *A video protocol of retroviral infection in primary intestinal organoid culture.* J Vis Exp, 2014(90): p. e51765.

69. Maru, Y., K. Orihashi, and Y. Hippo, *Lentivirus-Based Stable Gene Delivery into Intestinal Organoids.* Methods Mol Biol, 2016. **1422**: p. 13-21.

70. Fatehullah, A., S.H. Tan, and N. Barker, *Organoids as an in vitro model of human development and disease.* Nat Cell Biol, 2016. **18**(3): p. 246-54.

71. Cooper, H.S., et al., *Dysplasia and cancer in the dextran sulfate sodium mouse colitis model. Relevance to colitis-associated neoplasia in the human: a study of histopathology, B-catenin and p53 expression and the role of inflammation.* Carcinogenesis, 2000. **21**(4): p. 757-68.

72. Neufert, C., C. Becker, and M.F. Neurath, *An inducible mouse model of colon carcinogenesis for the analysis of sporadic and inflammation-driven tumor progression.* Nat Protoc, 2007. **2**(8): p. 1998-2004.

73. Moser, A.R., H.C. Pitot, and W.F. Dove, *A dominant mutation that predisposes to multiple intestinal neoplasia in the mouse.* Science, 1990. **247**(4940): p. 322-4.

74. Jackstadt, R. and O.J. Sansom, *Mouse models of intestinal cancer.* J Pathol, 2016. **238**(2): p. 141-51.

75. Nagy, A., *Cre recombinase: the universal reagent for genome tailoring.* Genesis, 2000. **26**(2): p. 99-109.

76. Hayashi, S. and A.P. McMahon, *Efficient recombination in diverse tissues by a tamoxifen-inducible form of Cre: a tool for temporally regulated gene activation/inactivation in the mouse.* Dev Biol, 2002. **244**(2): p. 305-18.

77. Engstrand, J., et al., *Colorectal cancer liver metastases - a population-based study on incidence, management and survival.* BMC Cancer, 2018. **18**(1): p. 78.

78. Flatmark, K., et al., *Twelve colorectal cancer cell lines exhibit highly variable growth and metastatic capacities in an orthotopic model in nude mice.* Eur J Cancer, 2004. **40**(10): p. 1593-8.

79. Khanna, C. and K. Hunter, *Modeling metastasis in vivo.* Carcinogenesis, 2005. **26**(3): p. 513-23.

80. Giavazzi, R., et al., *Metastatic behavior of tumor cells isolated from primary and metastatic human colorectal carcinomas implanted into different sites in nude mice.* Cancer Res, 1986. **46**(4 Pt 2): p. 1928-33.

81. Sachs, N. and H. Clevers, *Organoid cultures for the analysis of cancer phenotypes.* Curr Opin Genet Dev, 2014. **24**: p. 68-73.

82. Vlachogiannis, G., et al., *Patient-derived organoids model treatment response of metastatic gastrointestinal cancers.* Science, 2018. **359**(6378): p. 920-926.

83. O'Rourke, K.P., et al., *Transplantation of engineered organoids enables rapid generation of metastatic mouse models of colorectal cancer.* Nat Biotechnol, 2017. **35**(6): p. 577-582.

84. Daviaud, N., R.H. Friedel, and H. Zou, *Vascularization and Engraftment of Transplanted Human Cerebral Organoids in Mouse Cortex.* eNeuro, 2018. **5**(6).

85. Koeberle, S.C., et al., *Skepinone-L is a selective p38 mitogen-activated protein kinase inhibitor.* Nat Chem Biol, 2011. **8**(2): p. 141-3.

86. Selness, S.R., et al., *Discovery of PH-797804, a highly selective and potent inhibitor of p38 MAP kinase.* Bioorg Med Chem Lett, 2011. **21**(13): p. 4066-71.

87. Igea, A. and A.R. Nebreda, *The Stress Kinase p38alpha as a Target for Cancer Therapy.* Cancer Res, 2015. **75**(19): p. 3997-4002.

88. Simoes-Sousa, S., et al., *The p38alpha Stress Kinase Suppresses Aneuploidy Tolerance by Inhibiting Hif-1alpha.* Cell Rep, 2018. **25**(3): p. 749-760 e6.

89. Liu, R.Y., et al., *Activation of p38 mitogen-activated protein kinase is required for tumor necrosis factor-alpha -supported proliferation of leukemia and lymphoma cell lines.* J Biol Chem, 2000. **275**(28): p. 21086-93.

90. Annibaldi, A. and P. Meier, *Checkpoints in TNF-Induced Cell Death: Implications in Inflammation and Cancer.* Trends Mol Med, 2018. **24**(1): p. 49-65.

91. Montfort, A., et al., *The TNF Paradox in Cancer Progression and Immunotherapy.* Front Immunol, 2019. **10**: p. 1818.

92. Liu, T., et al., *NF-kappaB signaling in inflammation.* Signal Transduct Target Ther, 2017. **2**.

93. Sun, S.C., et al., *NF-kappa B controls expression of inhibitor I kappa B alpha: evidence for an inducible autoregulatory pathway.* Science, 1993. **259**(5103): p. 1912-5.

94. Ping, Z., et al., *Activation of NF-kappaB driven inflammatory programs in mesenchymal elements attenuates hematopoiesis in low-risk myelodysplastic syndromes.* Leukemia, 2019. **33**(2): p. 536-541.

95. Cha, H., et al., *A functional role for p38 MAPK in modulating mitotic transit in the absence of stress.* J Biol Chem, 2007. **282**(31): p. 22984-92.

96. Gavet, O. and J. Pines, *Progressive activation of CyclinB1-Cdk1 coordinates entry to mitosis.* Dev Cell, 2010. **18**(4): p. 533-43.

97. Karlsson-Rosenthal, C. and J.B. Millar, *Cdc25: mechanisms of checkpoint inhibition and recovery.* Trends Cell Biol, 2006. **16**(6): p. 285-92.

98. Schell, M.J., et al., *A multigene mutation classification of 468 colorectal cancers reveals a prognostic role for APC.* Nat Commun, 2016. **7**: p. 11743.

99. Miguel A. et al., Holland-Frei Cancer medicine 6th edition

100. Madden, K. and M.K. Kasler, *Immune Checkpoint Inhibitors in Lung Cancer and Melanoma.* Semin Oncol Nurs, 2019. **35**(5): p. 150932.

101. Wong, C.H., K.W. Siah, and A.W. Lo, *Estimation of clinical trial success rates and related parameters.* Biostatistics, 2019. **20**(2): p. 273-286.

102. Butler, D., *Translational research: crossing the valley of death.* Nature, 2008. **453**(7197): p. 840-2.

103. Suzuki, R., et al., *Strain differences in the susceptibility to azoxymethane and dextran sodium sulfate-induced colon carcinogenesis in mice.* Carcinogenesis, 2006. **27**(1): p. 162-9.

104. Mahler, M., et al., *Differential susceptibility of inbred mouse strains to dextran sulfate sodium-induced colitis.* Am J Physiol, 1998. **274**(3): p. G544-51.

105. Zheng, H., et al., *Establishing the colitis-associated cancer progression mouse models.* Int J Immunopathol Pharmacol, 2016. **29**(4): p. 759-763.

106. Breslin, S. and L. O'Driscoll, *Three-dimensional cell culture: the missing link in drug discovery.* Drug Discov Today, 2013. **18**(5-6): p. 240-9.

107. Fan, H., U. Demirci, and P. Chen, *Emerging organoid models: leaping forward in cancer research.* J Hematol Oncol, 2019. **12**(1): p. 142.

108. Ben-David, U., et al., *Genetic and transcriptional evolution alters cancer cell line drug response.* Nature, 2018. **560**(7718): p. 325-330.

109. Drexler, H.G., A.Y. Matsuo, and R.A. MacLeod, *Continuous hematopoietic cell lines as model systems for leukemia-lymphoma research.* Leuk Res, 2000. **24**(11): p. 881-911.

110. Pauli, C., et al., *Personalized In Vitro and In Vivo Cancer Models to Guide Precision Medicine.* Cancer Discov, 2017. **7**(5): p. 462-477.

111. Fleming, M., et al., *Colorectal carcinoma: Pathologic aspects.* J Gastrointest Oncol, 2012. **3**(3): p. 153-73.

112. Pereira, L., et al., *Inhibition of p38 MAPK sensitizes tumour cells to cisplatin-induced apoptosis mediated by reactive oxygen species and JNK.* EMBO Mol Med, 2013. **5**(11): p. 1759-74.

113. Yang, S.Y., et al., *Inhibition of the p38 MAPK pathway sensitises human colon cancer cells to 5-fluorouracil treatment.* Int J Oncol, 2011. **38**(6): p. 1695-702.

114. Gupta, J., et al., *Pharmacological inhibition of p38 MAPK reduces tumor growth in patient-derived xenografts from colon tumors.* Oncotarget, 2015. **6**(11): p. 8539-51.

115. de Witte, W.E.A., et al., *In vivo Target Residence Time and Kinetic Selectivity: The Association Rate Constant as Determinant.* Trends Pharmacol Sci, 2016. **37**(10): p. 831-842.

116. de Witte, W.E.A., et al., *The implications of target saturation for the use of drug-target residence time.* Nat Rev Drug Discov, 2018. **18**(1): p. 82-84.

117. Copeland, R.A., *The drug-target residence time model: a 10-year retrospective.* Nat Rev Drug Discov, 2016. **15**(2): p. 87-95.

118. Wentsch, H.K., et al., *Optimized Target Residence Time: Type I1/2 Inhibitors for p38alpha MAP Kinase with Improved Binding Kinetics through Direct Interaction with the R-Spine.* Angew Chem Int Ed Engl, 2017. **56**(19): p. 5363-5367.

119. Kotlyarov, A., et al., *MAPKAP kinase 2 is essential for LPS-induced TNF-alpha biosynthesis.* Nat Cell Biol, 1999. **1**(2): p. 94-7.

120. Brook, M., et al., *Regulation of tumour necrosis factor alpha mRNA stability by the mitogen-activated protein kinase p38 signalling cascade.* FEBS Lett, 2000. **483**(1): p. 57-61.

121. Cai, X., et al., *Inflammatory factor TNF-alpha promotes the growth of breast cancer via the positive feedback loop of TNFR1/NF-kappaB (and/or p38)/p-STAT3/HBXIP/TNFR1.* Oncotarget, 2017. **8**(35): p. 58338-58352.

122. Zhang, B., et al., *p38MAPK activation mediates tumor necrosis factor-alpha-induced apoptosis in glioma cells.* Mol Med Rep, 2015. **11**(4): p. 3101-7.

123. Cruceriu, D., et al., *The dual role of tumor necrosis factor-alpha (TNF-alpha) in breast cancer: molecular insights and therapeutic approaches.* Cell Oncol (Dordr), 2020. **43**(1): p. 1-18.

124. Schwitalla, S., et al., *Intestinal tumorigenesis initiated by dedifferentiation and acquisition of stem-cell-like properties.* Cell, 2013. **152**(1-2): p. 25-38.

125. Bulavin, D.V., et al., *Initiation of a G2/M checkpoint after ultraviolet radiation requires p38 kinase.* Nature, 2001. **411**(6833): p. 102-7.

126. Yuan, J., et al., *Cyclin B1 depletion inhibits proliferation and induces apoptosis in human tumor cells.* Oncogene, 2004. **23**(34): p. 5843-52.

127. Calonge, T.M. and M.J. O'Connell, *Turning off the G2 DNA damage checkpoint.* DNA Repair (Amst), 2008. **7**(2): p. 136-40.

128. Patnaik, A., et al., *A First-in-Human Phase I Study of the Oral p38 MAPK Inhibitor, Ralimetinib (LY2228820 Dimesylate), in Patients with Advanced Cancer.* Clin Cancer Res, 2016. **22**(5): p. 1095-102.

129. Vergote, I., et al., *A randomized, double-blind, placebo-controlled phase 1b/2 study of ralimetinib, a p38 MAPK inhibitor, plus gemcitabine and carboplatin versus gemcitabine and carboplatin for women with recurrent platinum-sensitive ovarian cancer.* Gynecol Oncol, 2020. **156**(1): p. 23-31.

130. Goldman, J.W., et al., *Phase 1 and pharmacokinetic study of LY3007113, a p38 MAPK inhibitor, in patients with advanced cancer.* Invest New Drugs, 2018. **36**(4): p. 629-637.